UNITED NATIONS UNIVERSITY
UNU-GTP
Geothermal Training Programme

Orkustofnun, Grensasvegur 9,
IS-108 Reykjavik, Iceland

Reports 2015
Number 14

PROCESSING AND JOINT 1D INVERSION OF MT AND TEM DATA FROM ALALLOBEDA GEOTHERMAL FIELD IN TENDAHO, NE-ETHIOPIA

Getenesh Hailegiorgis
Geological Survey of Ethiopia
P.O. Box 2302
Addis Ababa
ETHIOPIA
getenesh19@gmail.com, getegio@yahoo.com

ABSTRACT

Geophysical methods play a big role in geothermal resource exploration, for instance in revealing the electrical conductivity of the subsurface. Magnetotelluric (MT) and time domain electromagnetic resistivity methods are currently the most widely used resistivity methods. Resistivity is an important parameter because it is directly related to the physical properties of the reservoir.

Tendaho is one of the high-temperature geothermal fields in the Main Ethiopian Rift, NE-Ethiopia, and a promising area for geothermal development with respect to both its size and location. Alallobeda is one of the three prospects found in Tendaho geothermal field. Understanding the resistivity structure of the Alallobeda prospect could give a good understanding of the subsurface and enhance the possibility of developing the geothermal resource.

A total of 132 MT and Transient Electromagnetic (TEM) sounding pairs were acquired in 2014 and 2015 by the Geological Survey of Ethiopia (GSE) and the Italian consulting company Electro Consult (ELC) financed by the Icelandic International Development Agency (ICEIDA) and the Nordic Development Fund (NDF). Technical supervision for review and monitoring was done by Iceland GeoSurvey (ÍSOR). In this report, 54MT soundings were processed and almost the same number of TEM soundings. The soundings were1D inverted. TEM was used for static shift correction of the MT data from the same site. Some of the MT stations were inverted using MT data only based on a static shift correction given by the Italian consultant. The results are presented in the form of 1D models for individual stations, iso-resistivity maps and cross-sections. Three main resistivity layers were observed. The first is a thin layer of very low resistivity (< 10 Ωm) at shallow depth down to about 300 m b.s.l. which is correlated to sedimentary formation or a smectite- zeolite zone. Below the low resistivity a high-resistivity core appears with values between 100 and 1000 Ωm down to a depth of 1000 to 5000 m b.s.l. which can be correlated to the less permeable Afar Stratoid basalt series and high-alteration minerals like chlorite and epidote. Beneath the high-resistivity layer down to a depth of 5000 m b.s.l. a deep conductor is revealed that could be associated with the heat source.

1. INTRODUCTION

Geophysical methods, especially resistivity methods, and in particular magnetotellurics (MT) and Transient Electromagnetics (TEM) play an important role in geothermal exploration. The main reason is that resistivity is highly sensitive to temperature, salinity, porosity and geothermal alteration and it is directly related to the physical properties of the reservoir. Resistivity surveys identify variations in the electrical resistivity of the subsurface that are caused by different rock types and ground water. The main task of geophysical methods in geothermal exploration is to detect geothermal prospect, delineate geothermal resources and to further the understanding of their characteristics, as well as locating the exploitable reservoir and to help placing boreholes through which hot fluids can be extracted from depth. Geophysical exploration methods are different from other methods like geology and geochemistry in exploring geothermal resources because they use equipment that measure directly some physical parameters on the surface that reflect physical properties at depth in the earth´s crust (Flóvenz et al., 2012).

Geothermal exploration began in the Main Ethiopian Rift (MER) in 1969, carried out by the Ethiopian Government and the United Nation Development Programme (UNDP) (Bekele, 2012). In 1980, the Italian company Aquater began a detailed geological, geophysical and geochemical survey including a regional isotopic study in 1994 as well as monitoring of the deep Tendaho wells, drilled in the 1990s. The isotopic information highlighted that the recharge of the geothermal reservoir in the Tendaho Graben originates from the Western Escarpment (elevations above 2000 m) and excludes local recharge.

The geothermal prospects in Ethiopia lie in the MER system. Presently the total number of identified prospects is 23. Tendaho is one of the most promising geothermal areas in the MER system. A detailed geoscientific exploration survey was conducted in Alallobeda geothermal field, one of Tendaho´s three subfields in 2014-2015 by GSE and an Italian consulting company ELC, financed by ICEIDA and NDF. A part of the project was a resistivity survey, consisting of MT and TEM measurements. A total of 132 MT and 132 TEM soundings were done in 2014-2015, in addition to 27 MT soundings which had been done in 2013. The aim of the MT and TEM survey was to reveal the subsurface resistivity structure, to investigate whether a heat resource exists, to develop a conceptual geothermal model of the area and to propose sites of exploratory/production drilling targets.

In this project, geophysical methods applied in geothermal exploration, particularly electromagnetic methods, are discussed. In addition, TEM and MT soundings from the Alallobeda field in Tendaho are processed and 1D inverted.

2. THE TENDAHO GEOTHERMAL FIELD

2.1 Location of the study area

Tendaho geothermal field (see Figure 1) is located 600 km northeast of the capital city, Addis Ababa, in the central Afar depression. The area is bound between latitude 11°30´-12°N and longitude 41°00´-41°30´E. Alallobeda geothermal prospect is one of the three geothermal areas in Tendaho graben, the other two are Dubti and Ayrobera. Alallobeda geothermal prospect is located in the western part of the Tendaho Graben 15 km southwest of Dubti plantation, south-southeast of Logiya. It is characterized by flat plain land and a stratified mountainous range. The elevation of the area varies from 300 to 800 m.

The region´s population is mostly living of the breeding of camels, goats, sheep and donkeys. Due to the fertile alluvial soil and water supply of the Awash River, the most important economic activity during the past 4-5 decades has been the cultivation of cotton at Dubti, Det Bahri, Tangaye koma and Asayita plantation. Currently, the main agricultural product of the area is sugar and in some places of

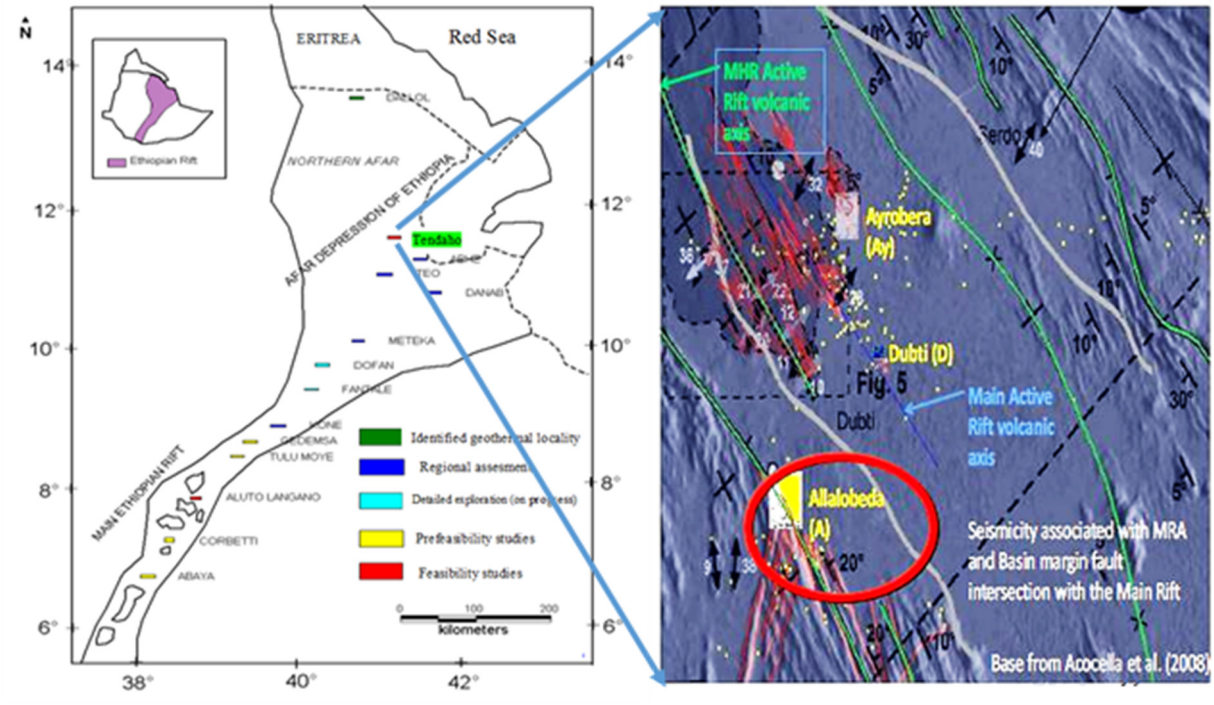

FIGURE 1: Location map of Tendaho

maize along the Awash River and utilizing water of the Awash Dam which is directed through canals at Dubti, Det Bahri, Tangaye Koma and Asayita.

An asphalt road from Addis Ababa branches at Semera to continue to Djibouti and Assab. Currently, the only sea-route out of Ethiopia is through Djibouti. Because of these circumstances, a temporary storage facility area has been built in Semera to minimize the cost for portal service. The traffic on the highway and the services needed in association with this have benefitted to the growth of the town Logiya. Semera, which started out as a road maintenance camp, has also served as the campsite for the geothermal exploration project since the 1990s. Semera became the capital city of the Afar region in 2004 and is growing fast.

The energy consumed by the rural population is mainly obtained from biomass fuel: wood from acacia trees, crop residue and camel and goat droppings. However, all four towns have electric supply, used primarily for household lighting and in the commercial sector. Dubti and Logiya are now connected to the EEPCo diesel generator in Semera. Dubti farm generates its own electricity for use at its ginnery and workshop and for air conditioning and lighting. Diesel fuel is used to generate power for irrigation and drainage pumping.

In the Afar region, the climate is of arid type and it is one of the hottest places in the country.

2.2 Geologic and tectonic setting of the Tendaho prospect area

The Afar depression is a part of the MER and is a triple junction (Figure 2) where three rifts separate three tectonic plates, the Nubian (Africa) plate, the Arabian plate and the Somalian plate. Two rifts are oceanic (Red Sea and Gulf of Aden rift) and one is continental (East African Rift). Tendaho is one of the high-temperature geothermal fields in the MER and a promising area for geothermal development with respect to its size and location. Several geothermal explorations have been carried out there since 1969.

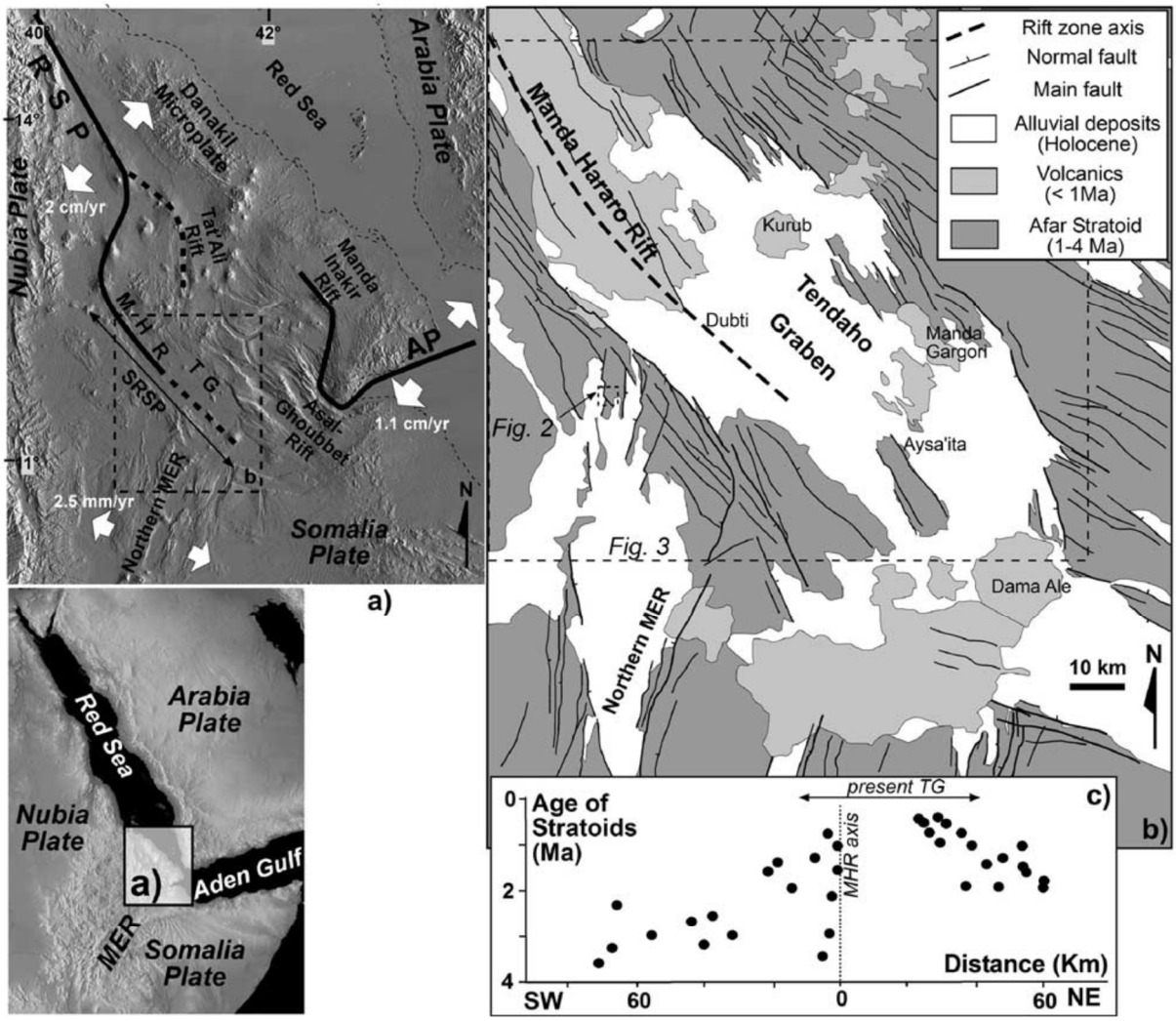

FIGURE 2. Regional setting of Afar region (bottom right): (a) General structure of the Afar triple junction. RSP, Red Sea propagator; SRSP, southern Red Sea propagator; AP, Aden Propagator; EAR, Erta Ale Range; MHR, Manda Hararo Rift; TG, Tendaho Graben; (b) Geology of Tendaho Graben area; (c) Projection of the age (in Ma) of the Afar Stratoid deposits along a NE-SW section perpendicular to the present MHR axis (age data from Barberi et al. (1975), Lahitte et al. (2001, 2003a, 2003b), and Kidane et al. (2003)); the figure is taken from Acocella et al., 2008

The northern Tendaho rift is tectonically characterized by open fissures and active faults which define a pattern of NW-SE elongated blocks with typical wave length of some hundreds of metres. In accordance with this tectonic trend, a general transtensive tectonic regime affects the area as pointed out by Aquater (1996) who carried out a micro-seismic survey. Satellite imagery and field observations show that the main lineament is NW-SE, indicating the prevalence of the Red Sea trend. At the western margin, NW-SE and NE-SW trending lineaments crisscross each other forming grid faults. Within the graben E-W and N-S trending structures are observed, though they are not prominent (Mamo and Bekele, 2014).

As shown in Figure 2, the Afar region is an area of active extensional tectonism and volcanism where the Red Sea, East African Rift system and Gulf of Aden Rift meet. Rifting in Afar began during lower Miocene on a continental arc where significant basaltic activity was probably in progress. The Afar depression is believed to have formed during the Pleistocene period with the formation of an axial ridge. Intense tensional tectonics affect the entire depression, thus, forming a complex mosaic of horsts and

grabens that are still active and contain localized sedimentary basins. From west to east, these are the Tendaho Graben, Dobi Graben, Gaggade Graben and Assal Graben (Megersa et al., 2006).

The northeast-trending Tendaho Graben, where the Alallobeda manifestations are located, has a width of about 50 km and joins the Ethiopian Rift close to Dama Ale the volcano west of Lake Abhe. The border of the graben consists of products of the Afar Stratoid Series (ASS) and the graben itself is filled with lacustrine and alluvial deposits and post-Stratoid basalt flows. The filling is overlain by recent volcanoes, including the historically active Kurub volcano (young products: 4,000-10,000 years) and Dama Ale (younger products: 2,500 years). In Tendaho Graben, under the recent sediments and the trachybasalt; the plagioclase pyric and perlite basalt rocks could be important aquifers due to their micro-fractures and close jointing and constitute reservoir formations for the geothermal system of Alallobeda.

There are different opinions on where the triple junction is located. Wolfenden (2003) states: "Magmatic segments of the main Ethiopian Rift terminate at the Tendaho Gda´ad discontinuity, which separates axial volcanic ranges, faults and fissures trending NW-SE, parallel with the incipient and diffuse Africa-Arabia plate boundary in central and northwest Afar, from north-northeast-trending magmatic segment in the MER. Termination of the MER at the Tendaho Graben Goba´da discontinuity marks the current Afro-Arabian triple junction. The current triple junction is therefore a broad sub-circular area of about 300 km in diameter centred on the Afar Depression, in which the three rift arms overlap, rather than a point".

In the vicinity of geothermal areas, the most identifiable point of intersection is near Alallobeda, where NNE-SSW-trending faults of the MER terminate and deflect into the major NW-SE-trending that bounds the graben on its southwest edge (Stimac et al., 2014).

2.3 Previous geophysical work

In 1969, a joint programme was performed by the Ethiopian government and the UNDP which included the study of the regional geology, geochemistry and hydrology of hot springs of the East African Rift System in Ethiopia (UNDP, 1973). In Tendaho, the first reconnaissance survey was done by UNDP and EIGS in 1973 (Megersa and Getaneh, 2006). Regional and semi-detailed geophysical studies were carried out in the Afar Depression and Tendaho geothermal field to find and investigate the deep structures and to delineate possible geothermal reservoirs. The geophysical methods included MT (e.g. Berktold, 1975), vertical electrical soundings (VES), a magnetic and gravity survey (e.g. Aquater, 1980) and others. Below, some of the surveys that have been done in Afar Depression are described.

An MT survey was carried out in the Afar region in 1971 to investigate the electrical resistivity distribution at depth (Berktold, 1975). The survey included 316 stations arranged on three profiles with a total length of 900 km. Profile I passes through the west of the plateau into the Afar Depression in an E-W direction (Dessie-Bati-Serdo) and crosses the study area. The results of the cross-structural model from profile I in the Afar Depression and under the western plateau have shown that the electrical resistivity layers vary from 200-500 Ωm in the uppermost kilometre, to 5-10 Ωm at about 15 km depth. The temperature at a depth of 15 km in the Afar Depression ranges from 800 to 1200°C corresponding to a mean gradient of about 60°C/km (Berktold, 1975).

In 1972 seismic measurements were made on five profiles, each 120-300 km in length. Along the profiles 350 stations were installed. Four of the profiles were located in the Afar lowland and one in the Ethiopian highlands. The interpretation shows a crustal thinning and upwelling of hot upper-mantle material underneath Afar (Berckhemer and Baier, 1975).

A gravity survey was carried out by Aquater (1980) with a total of 2086 stations. In the southeast centre of Tendaho (Dubti) plantation, a gravity low with a minimum value of -57 mgal was located. This may be caused by the thicker sediment accumulation in the graben which was also detected.

A ground magnetic survey by Aquater (also carried out in 1980) resulted in a map of the total magnetic field that shows a general magnetic low anomaly extending from NW to SE along the Tendaho Graben axis with minor anomaly perturbation, probably due to near surface inhomogeneities.

A micro-seismic survey was carried out by Aquater (1995) in the Tendaho Graben. It shows that the hypocentres of earthquakes are aligned along a line trending NW-SE, and are mostly located at 5 and 10 km depth.

A geophysical survey, which was carried out in 2013 (Kebede et al., 2013), reveals, based on impedance strike and tipper strike at different depth levels, that most of the stations show a general NW-SE strike direction which is coincident with the major trend of the Tendaho rift axis N25°W.

MT surveys were carried out in Tendaho by Lemma et al. (2012). The results show three major resistivity structures of variable thicknesses. Low resistivity associated with sediments and lateral flow of geothermal fluid or zeolite clay alteration zone (Aquater, 1996) is found near the surface. Below the conductive layers, higher resistivity of 8 Ωm is found, which can be correlated to Afar Stratoid basalt or epidote alteration zone, confirmed from alteration zones of wells TD1, TD2 and TD3 (Aquater, 1996). Then, a conductive layer is found at great depth, which can be correlated to magmatic melt associated with the heat source of the geothermal system.

2.4 Previous geochemical work

Water samples were collected from the Northern Afar Region for chemical and isotopic analyses (Gonfiantini et al., 1973). Later, gas samples were collected in fumaroles which can be found almost in the whole Ethiopian Rift valley. Craig (1977) conducted a regional chemical and isotopic study covering most of the Ethiopian Rift valley. Environmental isotopes of ^{18}O, D, tritium, ^{4}He, ^{14}C and ^{13}C were analysed and interpreted. The results of the exploration activities confirmed the existence of circulating high-temperature geothermal fluid at great depth that could be used for electrical power generation.

A radon soil gas survey was conducted in the Dubti geothermal prospect in 2010 with the help of the BGR (German Geological Survey) experts and led to the conclusion that the anomalous area is to the southeast of the drilled wells.

In 2012, another radon soil gas survey was conducted by Teclu and Mekonen (2013) in Ayrobera geothermal prospect and it identified anomalous structures trending NNE-SSW and in NNW-SSW. These structures also cross each other. The distribution of the thoron anomaly shows broken consecutive NNE-SSW, NNW-SSE and N-S directions.

The radon soil gas geochemical survey by Teclu and Mekonen (2013) also reveals the distribution of buried faults, joints or fractures. The investigation confirms that the anomalous values are concentrated along structures with NNE-SSW and N-S directions in the Alallobeda area.

Tendaho was the second area to be drilled after the Lakes district. In Tendaho geothermal field, six wells were drilled from 1993 to 1998 by the Italian government and Geological Survey of Ethiopia. Three deep wells namely TD1, TD2 and TD3 were drilled to a depth of 2196, 1811, and 1989 m, respectively. Three shallow wells, TD4, TD5 and TD6 were drilled to a depth of 466, 516 and 505 m, respectively. TD2, TD4, TD5 and TD6 are productive while TD1 and TD3 are non-productive. The elevation (m a.s.l.) of wells TD1, TD2, TD3, TD4, TD5 and TD6 is 365.9, 365.7, 366.8, 365.2, 366.3 and 366, respectively. The temperatures in the wells range from 200 to 270°C.

A preliminary production test and techno-economic study indicate that the shallow productive wells could supply enough steam to operate a pilot power plant of about 5 MWe and the potential of the deep reservoir is estimated to be about 20 MWe (Teklemariam and Kebede, 2010).

3. GEOPHYSICAL METHODS IN GEOTHERMAL EXPLORATION

3.1 Introduction

Geophysical methods are some of the most important methods in exploring geothermal areas. They use equipment that measure from the surface physical parameters which are directly related to physical properties or processes at depth in the earth´s crust. Combined with other geothermal exploration methods, their results can be used to find the size of geothermal fields and the likely successful drill sites.

The primary aim of geophysical exploration of geothermal areas is to:

- Find geothermal prospects;
- Outline drilling fields;
- Find the depth of reservoir;
- Locate aquifers and site wells;
- Estimate properties of the system.

Geophysical exploration is a fairly young scientific discipline which with regards to geothermal was developed in the mid twentieth century. With large advance in electronics, computer technology and model calculations during the past decades, it has developed more rapidly. Different parameters are measured in geophysical exploration, depending on the geophysical methods used.

Geophysical exploration methods can be classified into indirect and direct methods.

3.2 Indirect methods (structural methods)

The structural methods include gravity, magnetic and seismic measurements. Structural methods give information on anomalies caused by the associated geological formations or structures (e.g. fault and dykes).

Magnetics measurements: The spatial variations in the strength of the earth´s magnetic field are measured either on the ground or in an aeromagnetic survey. Surface bound magnetic surveys can trace narrow linear features like dykes and faults where the basement is covered with soil. In aeromagnetic surveys correlation has been found between magnetic anomalies and zones of intense hydrothermal alteration.

Magnetic methods are routinely employed for geothermal studies to outline structural lineaments which could be associated with faults and fractures as potential conduits for geothermal fluid circulations. Magnetic maps are used for structural purposes, locating intrusions, dykes, faults, buried lava and hydrothermally altered areas (Flóvenz et al., 2012).

Gravity surveys: Gravity anomalies are caused by spatial lateral density variations in the subsurface. Density variations are a result of compositional variations, porosity, differential weathering, hydrothermal alterations, fracturing of rocks and different structures. In geothermal areas possible sources of local gravity anomalies are dominantly hydrothermal alteration, intrusions and structural features, such as faults, calderas and basement structures (Nure, 2001).

Seismic surveys: Seismic methods can be divided into passive and active seismic methods depending on whether the source of seismic energy is natural or man-made.

Passive seismic methods detect seismic activity in the earth and can give information about velocity, attenuation, S-wave shadows, depth to the brittle/ductile boundary which indicates partial melt and magma chambers. Seismic activity that is studied in geothermal exploration is:

Ground noise (micro-seismicity) generated by the geothermal system through boiling.
Micro-earthquakes and earthquakes on active fault planes, hydraulic fracturing and tensile cracking of cooling intrusions.

An earthquake is a movement of crustal material along a new or pre-existing fault or fissure caused by a regional stress field. The non-elastic rupture is usually some tens or hundreds of metres for a small earthquake and can be regarded as a point source from a distance. The source location is called hypocentre and its projection to the surface of the earth is called epicentre.

A measure of the energy release (E) is the Richter M factor or magnitude which is on a logarithmic scale.

$$\log E = A + B \cdot M; B \approx 1.4 \quad (1)$$

An earthquake of magnitude 5 is about 10 times stronger (ten times more energy release) than an earthquake of magnitude 4. Earthquakes and micro-earthquakes give information on the stress field and the tectonic nature of the area where they occur. Stress is the internal force (per unit area) associated with strain which is the relative change in shape or size of an object due to an external applied force. Observation of seismic waves gives information on the properties of the transmission path from source to receiver (seismometer).

The location of a hypocentre is estimated from the arrival times of P-waves and S-waves at several stations. Thereby, it is assumed that the source is a point source and that the seismic wave travels through a transversely uniform earth (horizontal layers). In principle, an epicentre can be found from four P-arrival times. For increased accuracy, both S- and P-arrival times from three or more stations are used.

Some geothermal areas are characterized by an increased number of earthquakes, other show similar seismic activity as the region around the geothermal areas or even define a seismic gap (no seismic activity). Seismic studies have been used to investigate the regional tectonics where a geothermal area is located. As the tectonics and geological settings control the nature of most geothermal areas, the passive seismic method can deliver valuable information about the nature of geothermal systems (Hersir and Björnsson, 1991).

In general, passive seismic methods in geothermal exploration are used to map the location of the heat source, to map high cracking density zone, to determine the fluid zones, reservoir size and fault structure.

Active seismic methods detect sound velocity distribution and anomalies in the earth and its attenuation. The sound velocity distribution gives structural information about temperature and fluid-filled fracture zones (Hersir and Björnsson, 1991).

3.3 Direct methods

The direct methods include thermal and resistivity methods, including SP. Their success is based on them giving information on anomalies that are related to the geothermal activity. These are key methods in the exploration of geothermal systems, especially the resistivity methods.

Thermal methods: These are the most direct methods in geothermal exploration. The measurements can be carried out in the soil or in a borehole at a few metres depth. Temperature measurements in the boreholes delineate aquifers and can be used to estimate the temperature gradient which is a basic knowledge on a high-enthalpy geothermal system. Temperature measurements in the soil can also be useful in finding linear anomalies near hot springs and fumaroles, relating upflow to hidden linear structures.

Resistivity methods can be divided into DC methods and electromagnetic methods:

DC (direct current) resistivity methods are based on sending DC current into the earth and monitoring the potential signal it creates. There are several DC methods which have been used for decades in geothermal exploration. Some of these are Schlumberger and Wenner soundings, Head on profiling, Dipole soundings and profiling (Hersir and Björnsson, 1991).

Electromagnetic methods (EM): Using natural sources; magnetotellurics or MT is a passive method based on the natural electric field in the earth, created through natural variations in the earth's magnetic field. On the other hand, TEM is an active method based on creating a magnetic field in the earth and monitoring its response related to its decay as the source is turned off. Both methods are widely used in geothermal exploration, and the state of the art in modern geothermal research is the combination of these two methods.

S*elf-potential (SP)*: This is a passive method that measures the naturally occurring potential difference in the earth. It does not require electrical currents to be injected into the ground.

Geophysical well loggings and borehole methods: These are valuable tools for direct exploration and detection of physical parameters. Geophysical logging offers an opportunity to determine the composition, variability and physical properties of the rocks around the well enabling a proper understanding of the subsurface at a lower cost (Ofwona, 2010).

4. RESISTIVITY OF ROCKS

Resistivity of a material is defined as the electrical resistance in Ohms (Ω) between the opposite faces of a unit cube of the material (Kearey and Brooks, 1994). For a conducting cylinder of resistance R, length L and cross-sectional area A, the resistivity is given by:

$$\rho = \frac{RA}{L} \tag{2}$$

where ρ = Resistivity of the material (Ωm);
R = Resistance (Ω);
L = Length (m); and
A = Cross-sectional area (m^2).

The specific resistivity ρ depends on the material and is defined through Ohm´s law:

$$\boldsymbol{E} = \rho \boldsymbol{j} \tag{3}$$

where $\boldsymbol{E}$ = Electric field (V/m);
$\boldsymbol{j}$ = Current density (A/m^2).

The reciprocal of resistivity is conductivity ($1/\rho = \sigma$) and is given in Siemens per m.

The main electrical conduction mechanisms are mineral conduction, pore fluid conduction and surface conduction. Mineral conduction within the rock matrix itself is negligible in most cases, the rock matrix normally acts as an insulator except for very high temperatures > 800°C. The main electrical conduction mechanisms in geothermal fields are pore fluid conduction, which is conduction by dissolved ions in the pore fluid, and even more importantly, surface conduction by absorbed ions on the pore's surface.

Electrical resistivity of rocks depends on the parameters discussed briefly in the next subsections.

4.1 Porosity, permeability and the pore structure of the rock

Porosity and permeability are related to the properties of the rocks which are among others the number, size and connection of rock openings. Porosity is defined as the ratio between the pore volume and the total volume of a material.

$$\phi_t = \frac{V_V}{V_T} \tag{4}$$

where ϕ_t = Porosity;
V_V = Volume of void space (m^3);
V_T = Total or bulk volume of the material (m^3).

There are three main types of porosity (Hersir and Björnsson, 1991):

Intergranular: The pores are the spaces between grains or particles in a compact material like sediments and volcanic ash.
Joints-fissures: This is a net of fine fractures caused by tension and cooling of the rock common in igneous rocks and lava.
Vugular: As material is dissolved, big and irregular pores are formed and the material washed away. These can also be pores formed by gas as in volcanic rocks and limestone.

Pore space must be interconnected and filled with water so that the rock can conduct electricity. In all types of porosity there are large voids, called storage pores, and finer connected pores. Most of the resistance to electric current flow (and fluid flow) is in the connecting pores.

It has been observed in many cases that resistivity of water-bearing rocks varies approximately with the inverse square of the porosity. This empirical law, called Archie´s law (Archie, 1942), describes how resistivity depends on porosity if ionic conduction in the fluid dominates other conduction mechanisms in the rock.

$$\rho = \rho_w a \phi_t^{-n} \tag{5}$$

where ρ = Bulk (measured) resistivity (Ωm);
ρ_w = Resistivity of the pore fluid (Ωm);
ϕ_t = Porosity in proportion of total volume;
a = Empirical parameter, varies from < 1 for intergranular porosity to > 1 for joint porosity, usually around 1; and
n = Cementing factor, an empirical parameter, varies from 1.2 for unconsolidated sediments to 3.5 for crystalline rocks, usually around 2.

Archie´s law is valid if the resistivity of the pore fluid is in the order of 2 Ωm or less, but becomes less reliable if the resistivity is much higher (Flóvenz et al., 1985). However, Archie´s law seems to be a fair approximation when the conductivity is dominated by the saturating fluid (Árnason et al., 2000).

Permeability: This is the ability of the rock (material) to transmit water or fluid. It is the amount of fluid of a specified viscosity, under the influence of a given pressure, that passes through a sample having a certain cross-sectional area and thickness. It is mainly dependant on the size and shape of the pores in the materials.

4.2 Salinity of the water

Salinity is a measure of the total amount of salts in water or soil. Salts are highly soluble in surface and ground water and are transported with the water. Ground water may contain a variety of salts in the solution. Therefore, equivalent salinity is defined as the salinity of a NaCl-solution with the same resistivity as the particular solution. Mobility of the ions does not vary widely and equivalent salinity is

therefore close to true salinity. The bulk resistivity of a rock is mainly controlled by the resistivity of the pore fluid which is dependent on the salinity of the fluid. Figure 3 shows how conductivity changes with salinity.

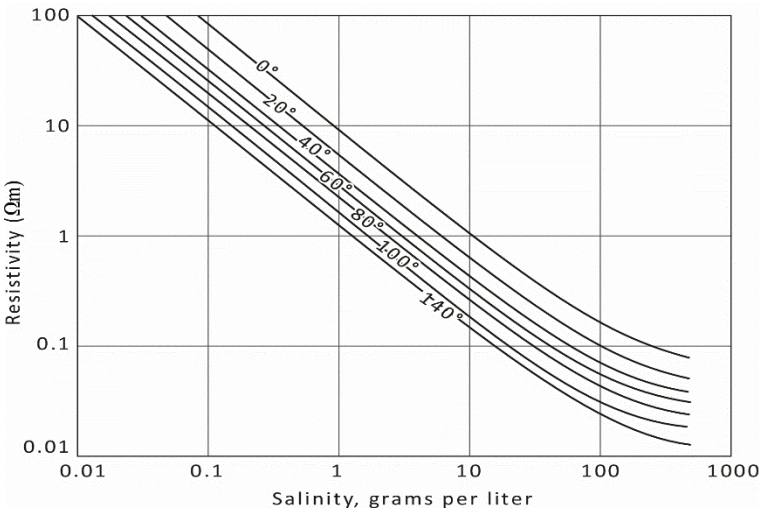

FIGURE 3: Electrical resistivity of NaCl solutions as a function of concentration and temperature (Flóvenz et al., 2012; based on Keller and Frischknecht, 1966)

In aqueous salt-solutions the ions of the solid separate and start to move freely in the solution. If the amount of dissolved solids in the pore fluid increases, the conductivity also increases as shown in Figure 3. Therefore, the conductivity of a solution is a function of salinity and the mobility of the ions present in the solution. The mobility of the ions depends on temperature (viscosity) and on concentration. The conductivity of a solution can be expressed by the following equation (Hersir and Björnsson, 1991):

$$\sigma = F(c_1 q_1 m_1 + c_2 q_2 m_2 + \cdots) \quad (6)$$

where σ = Conductivity (S/m);
F = Faraday´s number (9.65 x10^4 C/mole);
c_i = Concentration of ions;
q_i = Valance of ions**;** and
m_i = Mobility of different ions.

4.3 Temperature

At moderate temperatures, between 0 and 200°C, resistivity of aqueous solutions decreases with increasing temperature as shown on Figure 4. This is because of increasing mobility of ions at increasing temperature caused by a decrease in the viscosity of the water. Dakhnov (1962) has described this relationship:

$$\rho_w = \frac{\rho_{wo}}{1 + \alpha(T - T_o)} \quad (7)$$

where ρ_{wo} = Resistivity of the fluid at temperature T_0 (Ωm);
α = Temperature coefficient of resistivity $(°C^{-1})$ (≈ 0,023 $°C^{-1}$ for T_o = 25 °C).

At high temperatures, a decrease in the dielectric permittivity of the water results in a decrease in number of dissociated ions in the solution. Above 250°C the resistivity of the fluid starts to increase (Quist and Marshall, 1968).

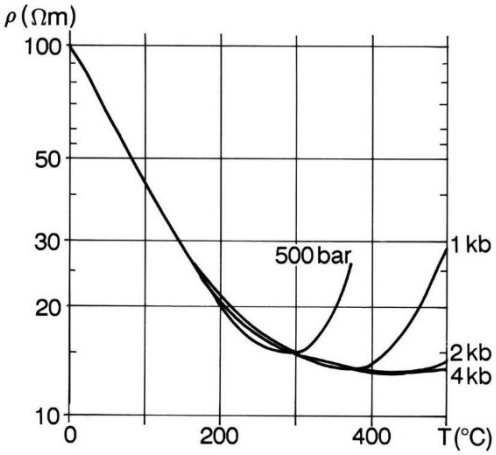

FIGURE 4: Electrical resistivity of NaCl solution as a function of temperature at different pressures (Hersir and Björnsson, 1991; based on Quist and Marshall, 1968)

4.4 Water rock interaction and alteration mineralogy

Water-rock interaction is the interaction of water with rocks which not only extracts the heat but also causes changes in the chemistry of both the water and the rock. Alteration minerals are formed through hydrothermal alteration processes when hydrothermal water reacts with the rock.

The alteration processes and the resulting type of alteration minerals are dependent on the type of primary minerals and the chemical composition of the geothermal fluid and temperature (see right part of Figure 5). The intensity of the alteration is further dependent on the contact time and texture of the host rocks. Alteration intensity is normally low for temperatures below 50°C. At temperatures below 220°C, low-temperature zeolites and the clay minerals smectite are formed. Smectite has hydrated and loosely bound cations between the silica plates, making the mineral conductive and provides it with a high cation exchange capacity (Árnason et al., 2000).

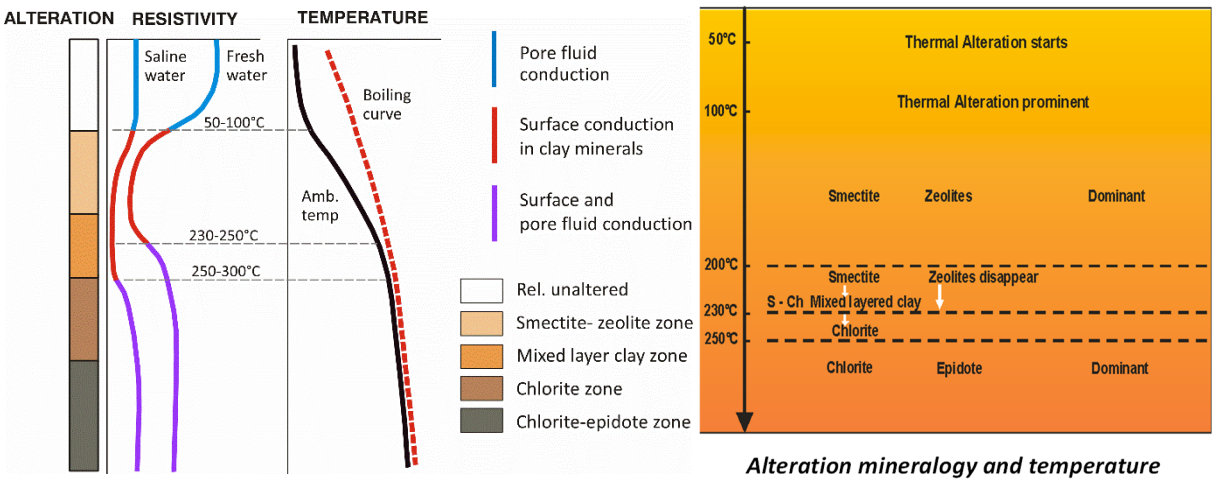

FIGURE 5: The general resistivity structure of a high-temperature geothermal system in basaltic environment showing resistivity variations as a function of alteration and temperature (Flóvenz et al., 2012)

In the temperature range from 220 to about 240-250°C, the low-temperature zeolites disappear and smectite is transformed into chlorite in a transition zone, the so-called mixed-layered clay zone, where smectite and chlorite coexist in a mixture. At about 250°C smectite disappears and chlorite is the dominant mineral, marking the beginning of the chlorite zone. Hence, with increased resistivity, since chlorite minerals have cations that are fixed in a crystal lattice, the mineral is much more resistive. At still higher temperature about 250-270°C, epidote becomes abundant in the so-called chlorite-epidote zone (Árnason et al., 2000).

As shown in the left part of Figure 5, in high-temperature areas in basaltic environment the resistivity in the upper-most part of the subsurface is relatively high and the main conduction mechanism is pore fluid conduction, no alteration is found. Resistivity decreases as the temperature increases and smectite and zeolite become the dominant alteration minerals (temperature > 100°C). The conduction mechanism is surface conduction in clay minerals. Below the smectite alteration, chlorite and mixed-layered clay dominate and the resistivity increases again. This is because chlorite has bound cations that are fixed in the crystal lattice making them resistive. Here, surface and pore fluid conduction are dominant. At greater depth where epidote becomes dominant, the resistivity is high due to the crystal lattice formation, the conduction mechanism is surface and pore fluid conduction.

Resistivity is directly proportional to the alteration minerals and not necessarily related to temperature, since the geothermal system might be fossil.

5. MT AND TEM RESISTIVITY METHODS IN GEOTHERMAL EXPLORATION

5.1 Basic theory of electromagnetic methods

Electromagnetic (EM) methods are commonly used in surface exploration of geothermal areas to determine the spatial distribution of the electrical conductivity in the subsurface. The MT method has found to be the most effective EM method in delineating conductivity at great depth. The TEM method is used to investigate the resistivity structure at shallow depths and also for static shift correction of MT data.

The behaviour of electromagnetic fields at a given frequency can de described by Maxwell´s equations in a conductive media:

$$\boldsymbol{\nabla} \times \boldsymbol{E} = -\frac{\partial \boldsymbol{B}}{\partial t} \tag{8}$$

$$\boldsymbol{\nabla} \times \boldsymbol{H} = \boldsymbol{j} + \frac{\partial \boldsymbol{D}}{\partial t} \tag{9}$$

$$\boldsymbol{\nabla} \cdot \boldsymbol{B} = 0 \tag{10}$$

$$\boldsymbol{\nabla} \cdot \boldsymbol{D} = \eta \tag{11}$$

where **E** = Electric field (Vm^{-1});
B = Magnetic induction (T);
D = Electric displacement (Cm^{-2});
$\boldsymbol{j}$ = Electric current density (Am^{-2});
η = Electric charge density owing to free charges (Cm^{-3});
$(\nabla \times)$ = Curl and $(\nabla \cdot)$ = div.

A harmonic dependency of the oscillating electromagnetic fields **E** and **H** is assumed as: $\sim e^{i\omega t}$. For a linear and isotropic media, the vector fields in Maxwell's equations (Equations 8-11) can be related through the constitutive relationships, $\boldsymbol{j} = \sigma \boldsymbol{E}$, $\boldsymbol{B} = \mu \boldsymbol{H}$ and $\boldsymbol{D} = \varepsilon \boldsymbol{E}$.

According to Snell's law, we have:

$$\frac{1}{v_o} \sin \theta_i = \frac{1}{v} \sin \theta_t$$

V_o and V are the velocities in the air and in the half-space, respectively and can be described as:

$$V_o = \frac{1}{\sqrt{\varepsilon \mu}} \text{ and } v = \sqrt{\frac{2\omega}{\mu \sigma}}$$

Hence:

$$\sin \theta_t = \sin \theta_i \sqrt{\frac{2\varepsilon\omega}{\sigma}} \text{ and } \frac{2\varepsilon\omega}{\sigma} < 10^{-3}$$

θ_t is therefore close to zero; incident plane waves travel vertically downwards for all angles of incidence θ_i.

5.1.1 MT methods

MT is a passive EM method that measures the fluctuations in the natural electric field **E** and magnetic field **B** in orthogonal directions at the surface of the earth to determine the electrical conductivity distribution of the earth at depth ranging from a few hundred metres to tens of kilometres. The

fundamental MT theory was first introduced by Tikhonov (1950, reprinted 1986) and, in more details, by Cagniard (1953).

The depth of penetration of the EM wave into the earth is inversely proportional to rock conductivity. In a uniform earth, **E** and **H** decay exponentially with depth; the more conductive the earth, the less is the penetration.

At the depth $\delta(T)$, the so called skin depth, EM wave are attenuated to e^{-1} of their amplitudes at the surface of the earth. Hence, in MT studies, one electromagnetic skin depth is generally equated with the penetration depth of electromagnetic wave into the earth. In MT studies of the earth, μ is usually the free space value ($\mu_o = 4\pi \times 10^{-7} Hm^{-1}$) and the skin depth can be written as:

$$\delta(T) \approx 500\sqrt{T\rho_a}\ (\text{m}) \qquad (12)$$

where, $\delta(T)$ = Electromagnetic skin depth in m for a given period T (s); and
ρ_a = Apparent resistivity, or the average resistivity of an equivalent uniform half space.

From the above equation we can conclude that for a given period, the depth achieved by the EM wave will be dictated by the average conductivity of the overlying earth that is penetrated (Simpson and Bahr, 2005).

AMT and MT techniques are essentially the same, differing only in the frequency range and the different sources. MT Phoenix equipment acquires data in the frequency range from 400-0.0000129 Hz. AMT acquires data in the frequency range of about 100-10.000 Hz (roughly the range of human hearing, hence the audio designation). Therefore, MT is used for deeper and AMT for shallow investigation.

Magneto hydrodynamic processes within the Earth´s outer core generate the greater part of the Earth´s magnetic field. It is the superimposed, more transient, lower amplitude fluctuation of external origin that MT sounding seeks to exploit. The power spectrum of these plummets is in the range 0.5-5 Hz frequency, minimizing at frequency of ~1 Hz. So for MT the frequency between 0.5-5 Hz is called the dead band frequency, the MT soundings lack data quality in this range. For AMT the dead band frequency around $\sim 1 - 10$ kHz .

Source of MT sounding: Figure 6 shows one of the sources of MT soundings. In the MT methods time variations in the earth´s magnetic field are used to probe the surface resistivity structure. The earth´s EM field contains a wide frequency spectrum, high frequencies >1 Hz (periods shorter than 1 second) are due to thunderstorms near the equator which are distributed in the form of guided waves between

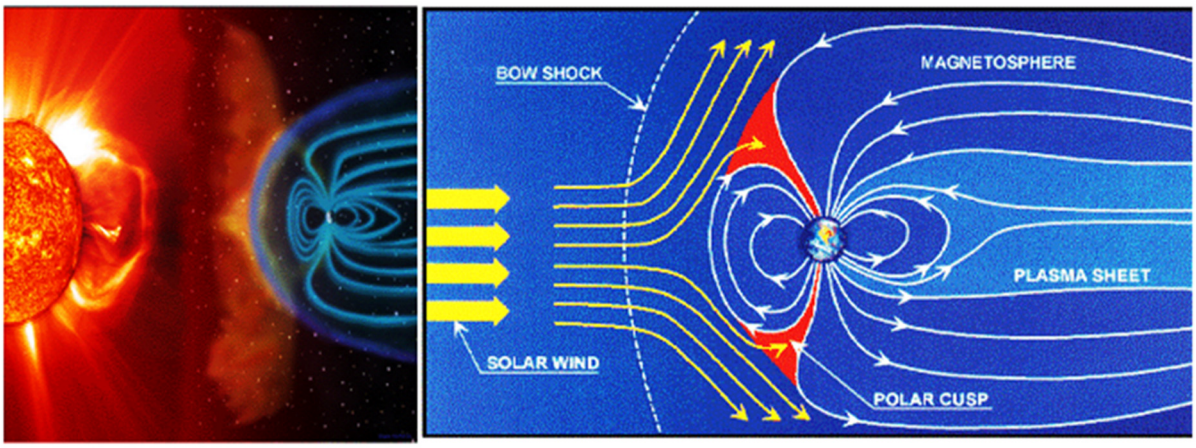

FIGURE 6: Interaction of solar wind with the magnetosphere, source of low frequency natural EM (Adapted from Sky and Telescope (2015) and CNES Scientific Missions (2015))

the earth and ionosphere. The lower frequencies <1 Hz (periods longer than 1 second) are generated by ionospheric and magnetospheric currents caused by plasma interfering with the earth's magnetic field.

The largest geomagnetic field variations on the order of a few hundred nT occur during magnetic storms, which happens due to a sporadic increase in the rate at which plasma is ejected from the sun. Magnetic storms last for several days, they become visible at high latitudes in form of Aurora Borealis and Aurora Australis, or northern and southern lights, respectively (Simpson and Bahr, 2005). Aurora is a natural light displayed in the sky and it is associated with solar wind, a flow of charged particles continuously flowing away from the sun. The earth´s magnetic field traps these particles, many of which travel toward the poles where they are accelerated towards the earth (Lemma, 2010).

The MT method depends on the penetration of electromagnetic energy into the earth. The measurements are absolute and the apparent resistivity calculations from MT measurements are accurate for the true resistivity values. Their interpretation gives true resistivity values and true depths, not just anomalies. Depth interpretation based on MT data is therefore much more definitive than interpretation of gravity or magnetic data (Vozoff, 1972).

Impedance: If the electromagnetic wave propagates through a homogeneous and isotropic medium, the electric and magnetic field vectors are orthogonal. The ratio of the orthogonal components of the electric and magnetic field are derived from Maxwell's equations. The characteristic impedance is denoted by **Z**. The impedance tensor elements describe the relationship between the electric and magnetic fields in matrix form.

$$\begin{pmatrix} E_x \\ E_y \end{pmatrix} = \begin{pmatrix} Z_{xx} & Z_{xy} \\ Z_{yx} & Z_{yy} \end{pmatrix} \begin{pmatrix} H_x \\ H_y \end{pmatrix} \tag{13}$$

$$E_x(\omega) = Z_{xx}(\omega)H_x(\omega) + Z_{xy}(\omega)H_y(\omega) \tag{14}$$

$$E_y(\omega) = Z_{yx}(\omega)H_x(\omega) + Z_{yy}(\omega)H_y \tag{15}$$

$$Z_{xy} = \frac{E_x}{H_y} = \frac{i\omega\mu_o}{k} \tag{16}$$

$$Z_{yx} = \frac{E_y}{H_x} = \frac{-i\omega\mu_o}{k} \tag{17}$$

where Z_{xy}, Z_{yx} = Characteristic impedance elements;
ω = Angular frequency ($2\pi f$) where f is frequency (Hz);
k = $\sqrt{i\omega\mu(i\omega\varepsilon + \sigma)}$, stands for the propagation constant.

Assuming $\sigma \gg \omega\varepsilon$, the wave propagation constant k can be simplified to the quasi-stationary approximation $k = \sqrt{i\omega\mu\sigma}$. Substituting this into Equations 16 and 17 gives:

$$Z_{xy} = \frac{E_x}{H_y} = \frac{i\omega\mu}{\sqrt{i\omega\mu\sigma}} = \sqrt{i}\sqrt{\omega\mu\rho} = \sqrt{\omega\mu\rho}\, e^{i\pi/4} \tag{18}$$

$$Z_{yx} = \frac{E_y}{H_x} = \frac{-i\omega\mu}{k} = -Z_{xy} \tag{19}$$

This shows that there is phase difference of $\pi/4$ or 45° between E_x and H_y as shown in Figure 7. If the earth is homogenous and isotropic, the true resistivity is related to the characteristic impedance using Equation 18 through the relation:

$$\rho = \frac{1}{\omega\mu}\left|Z_{xy}\right|^2 = \frac{1}{\omega\mu}\left|Z_{yx}\right|^2 \tag{20}$$

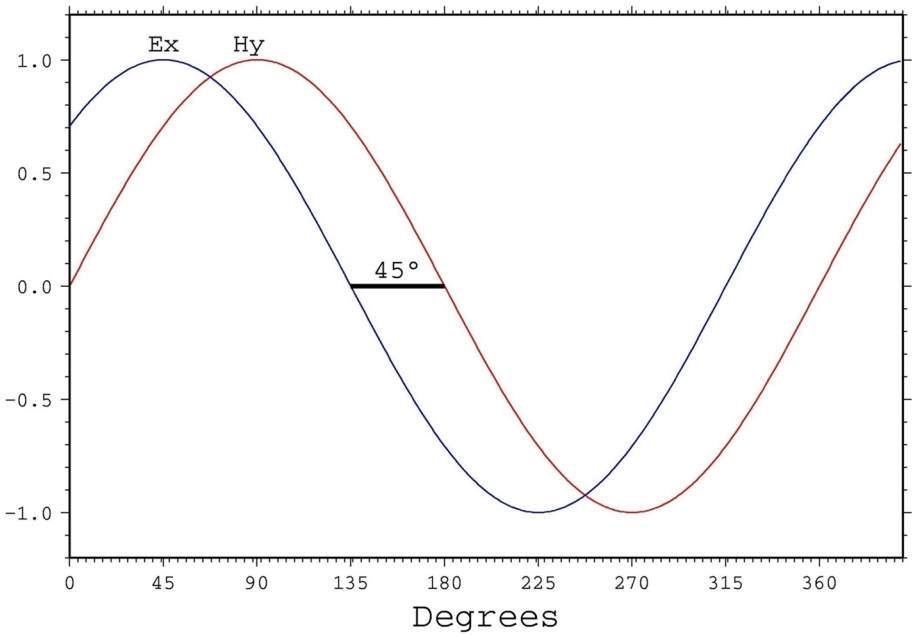

FIGURE 7: The phase difference between the **E** and **H** field
for homogenous half space

In general:

$$\rho = \frac{1}{\omega\mu}|Z|^2 \tag{21}$$

Equation 21 can be re-written using magnetic field intensity $\boldsymbol{B} = \mu\boldsymbol{H}$ in the unit Tesla (T) and electric field $\boldsymbol{E}$ in the practical unit mV/km. For a homogeneous earth, ρ and Z are independent of T:

$$\rho = \frac{T}{2\pi\mu} = \left|\frac{E_x 10^{-6}\mu}{B_y 10^{-9}}\right|^2 = \frac{T\mu}{2\pi}\left|\frac{E_x}{B_y}\right|^2 10^6 = 0.2T\left|\frac{E_x}{B_y}\right|^2 \tag{22}$$

or

$$\phi = arg(Z) = {}^{\pi}/_{4} = 45° \tag{23}$$

For a non-homogeneous earth, ρ and Z depend on T and the apparent resistivity (ρ_a) and phase (ϕ_a) are defined as:

$$\rho_a(T) = 0.2T|Z_o|^2 = 0.2T\left|\frac{E_x}{B_y}\right|^2 \quad and\ the\ phase \quad \phi_a(T) = arg(Z_o) \neq 45° \tag{24}$$

where Z_o = Impedance at the surface.

Impedance tensor: This tensor describes the relationship between the orthogonal electric and magnetic field at a given frequency:

$$\begin{bmatrix} E_x \\ E_y \end{bmatrix} = \begin{bmatrix} Z_{xx} & Z_{xy} \\ Z_{yx} & Z_{yy} \end{bmatrix} \begin{bmatrix} H_x \\ H_y \end{bmatrix} \tag{25}$$

Depending on the spatial distribution of the electrical conductivity the impedance tensor components reduce to a particular expression. The spatial distribution, also called geo-electric dimensionality, can be classified as 1D, 2D or 3D.

Definition of apparent resistivity – non-homogenous media
1D impedance tensor: For a 1D layered earth the resistivity distribution varies only with depth. The diagonal element of the impedance tensor Z_{xx} and Z_{yy} are zero and the off-diagonal elements of the impedance tensor Z_{xy} and Z_{yx} are equal in magnitude but opposite in sign. Therefore, from Equation 25 the impedance tensor for 1D can be written as:

$$Z_{1D} = \begin{vmatrix} 0 & Z_{xy} \\ Z_{yx} & 0 \end{vmatrix} \tag{26}$$

The corresponding apparent resistivity and phase for 1D earth can be defined as:

$$\rho_a = \frac{1}{\mu\omega}|Z|^2 \text{ and } \phi_a = \tan^{-1}\left(\frac{ImZ}{ReZ}\right) \tag{27}$$

The impedance phase gives additional information about the resistivity structure. It can be determined as the tangent inverse of the ratio of imaginary to real component of the tensor.

2D impedance tensor: For a 2D earth, the resistivity is constant in one horizontal direction but varies in the other horizontal direction and with depth. The direction along which the resistivity is constant is known as the geo-electrical strike or electromagnetic strike direction. The diagonal elements of the impedance tensor are equal to zero, but the off-diagonal elements are different in magnitude $\left(Z_{xy} \neq -Z_{yx}\right)$.

If the x-direction is parallel to the strike and the y-direction is perpendicular to it, the diagonal elements of the impedance tensor become zero $\left(Z_{xx} = Z_{yy} = 0\right)$ and the impedance tensor can be written as:

$$Z_{2D} = \begin{vmatrix} 0 & Z_{xy} \\ Z_{yx} & 0 \end{vmatrix} \tag{28}$$

where $Z_{xy} = Z_{TE} = \frac{E_x}{H_y}$; and $Z_{yx} = Z_{TM} = \frac{E_y}{H_x}$

For the 2D electrical resistivity structure, the magnetic field splits into two independent modes:

1. Transverse magnetic (TM) mode: the magnetic field is parallel to the electric strike direction;
2. Transverse electric (TE) mode: the electric field is parallel to the electric strike direction.

In TM mode or B-polarization the magnetic field is polarized parallel to the electromagnetic strike, in TE mode or E-polarization the electric field is polarized parallel to the electromagnetic strike. In TM mode or B-polarization the electric field is polarized perpendicular to the electromagnetic strike, and in TE mode or E-polarization the magnetic field is polarized perpendicular to the electromagnetic strike as shown in Figure 8.

3D impedance tensor: The resistivity varies in all three directions ($\rho = \rho(x, y, z)$). In this case the impedance tensor takes the general form ($Z_{xx} \neq Z_{yy} \neq 0$ and $Z_{xy} \neq Z_{yx}$). The impedance tensor in Equation 25 can be written as:

$$Z_{3D} = \begin{vmatrix} Z_{xx} & Z_{xy} \\ Z_{yx} & Z_{yy} \end{vmatrix} \tag{29}$$

There exists no rotational direction where both diagonal elements of the impedance tensor or any component of the tipper vector will vanish. If the tensor elements are non-zero there is a resistivity boundary.

Skew: This is the ratio of the amplitude of the diagonal impedance elements to the off-diagonal impedance elements. Skew is another measure of 3D dimensionality. It does not change with rotation of the coordinates.

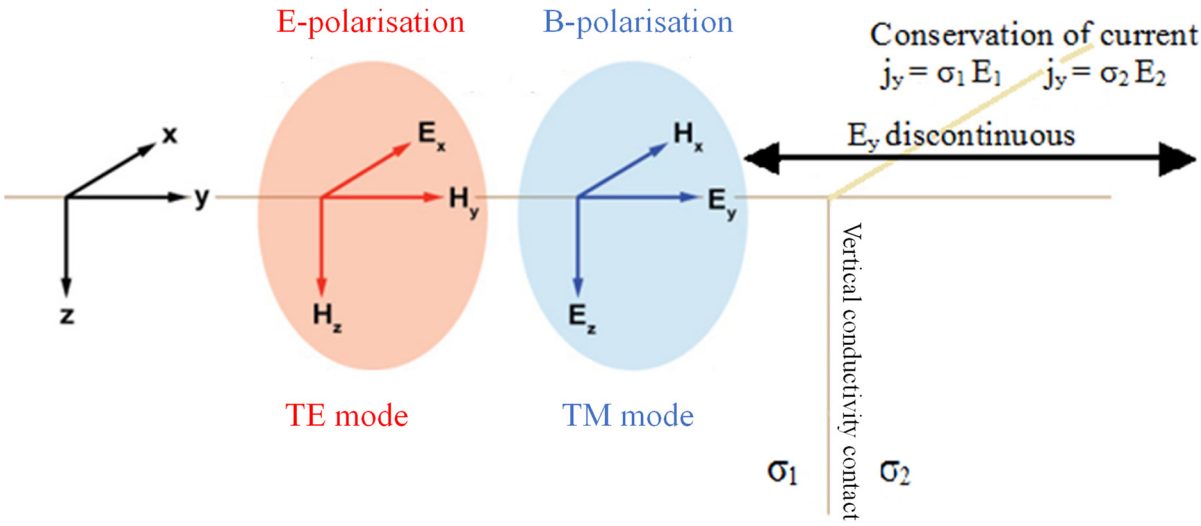

FIGURE 8: 2D model and the concept of polarizations in magnetotelluric (Teklesenbet, 2012)

$$Skew = \left| \frac{Z_{xx} + Z_{yy}}{Z_{xy} - Z_{yx}} \right| \tag{30}$$

In 1D and 2D cases, the skew should be close to zero. Large deviations from zero are an indicator of three-dimensionality. Typical values below 0.2 were taken to indicate that the response could be interpreted in a 1D or 2D manner (Simpson and Bahr, 2005; Berdichevsky and Dmitriev, 2002).

5.1.2 TEM methods

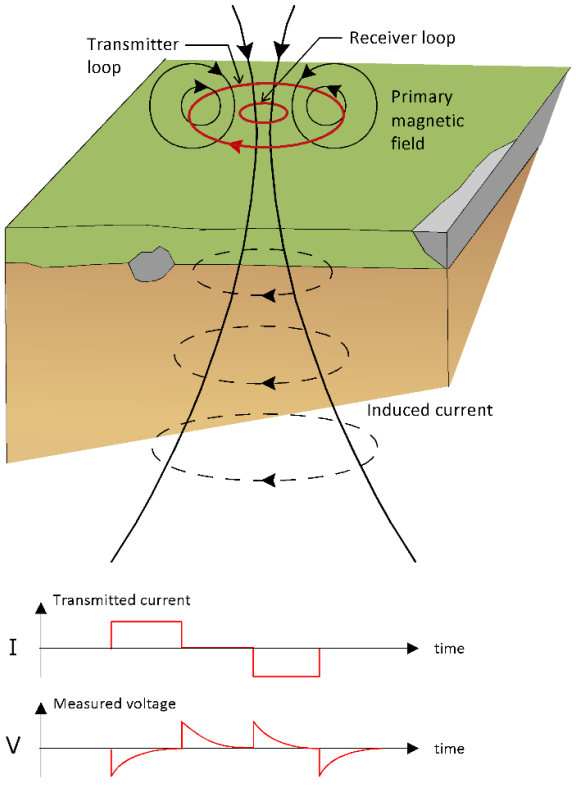

FIGURE 9: The central loop TEM sounding configuration (Flóvenz et al., 2012; based on Hersir and Björnsson, 1991)

TEM is an active EM geophysical exploration method used in exploration of geothermal resources. TEM surveys are also very common in mineral exploration, ground water surveys and in environmental mapping. It is used throughout the world in both onshore and offshore applications. Generally, TEM methods are able to determine subsurface electrical properties, but they are also sensitive to subsurface magnetic properties in applications like unexploded ordnance (explosive weapons like bombs, shells, land mines, etc.) detection and characterization.

In the volcanic zones where the surface is mostly covered by lava, current injection into the ground is a major problem when using Schlumberger soundings. In the TEM method no current is injected into the ground, but into a source loop on the surface. The EM method is classified as frequency domain or time domain, depending on the measuring techniques employed. Time domain electromagnetic methods (TEM) are further classified as grounded or loop source methods depending on how the source field is introduced into the ground (Kebede, 2001).

The setup of the central-loop TEM method is shown in Figure 9. A loop of wire is placed on the ground

and a constant magnetic field of known strength is built up by transmitting a constant current into the loop. The current is then turned off abruptly. The decaying magnetic field induces an electrical current in the ground. This current induces a secondary magnetic field which decays with time (Figure 9). The decay rate of the secondary magnetic field is monitored by measuring the voltage induced in a receiver coil (or small loop) at the centre of the transmitter loop. The current distribution and the decay rate of the secondary magnetic field depends on the resistivity structure of the earth. The decay rate, recorded as a function of time after the current in the transmitter loop is turned off, can therefore be interpreted in terms of the subsurface resistivity structure.

The depth of penetration in central loop TEM-soundings is dependent on how long the induction in the receiver coil can be traced in time before it is drowned in noise. At late times, the induced voltage in the receiving coil on homogeneous half space of conductivity σ is approximately given by (Árnason, 1989).

$$V(t,r) = I_o \frac{C(\mu\sigma r^2)^{3/2}}{10\pi^{1/2}t^{5/2}} \tag{31}$$

where C $= A_r n_r A_s n_s \frac{\mu_o}{2\pi r^3}$;
A_r = Cross-sectional area of the receiver coil (m^2);
n_r = Number of turns in receiver loop;
A_s = Area of transmitting loop (m^2);
n_s = Number of turns in transmitter loop;
t_r = Time elapsed after the current in the transmitter is turned off (s);
μ = Magnetic permeability (H/m);
V(t,r) = Transient voltage (V);
r = Radius of the transmitter loop (m);
I_o = Current in the transmitter loop (A).

Substitution of $\sigma = {}^1/_\rho$ gives the late time apparent resistivity as a function of time after the current is turned off at the transmitter:

$$\rho_a = \frac{\mu}{4\pi}\left[\frac{2\mu I_o A_r n_r A_s n_s}{5t^{5/2}V(t,r)}\right]^{2/3} \tag{32}$$

where ρ_a = Late time apparent resistivity (Ωm).

The apparent resistivity curve is inverted in terms of a horizontally layered Earth´s model with homogenous and isotropic layers (1D model). The model helps to interpret the data because both the resistivity and thickness of the layers can vary in the inversion. The most common 1D interpretation is Occam (minimum structure) inversion of each sounding. In Occam inversion, the smooth variations are approximated by numerous thin layers of fixed thicknesses and the data is inverted for the values of the resistivity (Flóvenz et al., 2012).

Central loop TEM-sounding method has several advantages over conventional DC-sounding methods:

1. The transmitter couples inductively to the earth and no current has to be injected into the ground. This is of great importance in areas where the surface is highly resistive (Árnason, 1989).
2. The fact that the monitored signal is a decaying magnetic field rather than an electric field at the surface makes the results much less dependent on local resistivity conditions at the receiver site (Sternberg et al., 1988). Distortion due to local resistivity inhomogeneities at the receiver site can be a severe problem in DC-soundings as well as in MT soundings (Árnason, 1984).
3. It is less sensitive to lateral resistivity variations than the DC methods. The reason is that in the TEM method, the current induced in the ground can be visualized as a diffuse current ring which at early times, after the current in the transmitter loop is turned off, simulates the current in the transmitter loop (Hoversten and Morrison, 1982). With time this current ring diffuses downwards and outwards resulting in an increased depth of penetration with time. The monitored signal at

the surface is primarily dependent on the resistivity structure inside the diffuse current ring. The central loop TEM-soundings are thus much more downwards focused than DC-soundings, where increased depth of penetration is obtained by increasing the distance between the current injection electrodes and the receiver dipole, making the monitored electric field dependent on a much large volume of rocks.

4. TEM field survey needs less man power and is faster. It gives a more detailed model of the geothermal system. However, TEM soundings are more sensitive to man-made noise than DC methods (like Schlumberger).

6. DATA PROCESSING AND INVERSION OF TEM AND MT

6.1 Inversion

Inversion is used to estimate the model parameters using the measured data. To solve the inversion problem one has to know how to calculate the forward problem. At first a starting model is chosen and the forward algorithm calculates the response. If the calculated response does not fit with the measured data, an inversion algorithm improves the model in order to improve the fit with the measured data.

Forward modelling is a process of predicting data based on some physical or mathematical model with a given set of model parameters. Forward modelling is an important part of the inversion method, and it has to be accurate, fast and reliable. The inversion process uses forward modelling to compute the sensitivity matrix and the response for calculating the misfit. Inversion is used to estimate the quality of the predicted model parameters and to determine which model parameters are the most important in constraining the estimated model parameters. The most commonly used inversion method for geoelectric soundings is the least-square inversion method. After each iteration step we get a sensitivity matrix which gets us nearer the exact model, characterized by the chi-square (χ).

6.2 TEM data processing and inversion

The TEM data in Alallobeda were acquired using two instruments from different manufacturing companies, Zonge GDP-32 and Phoenix V8 TEM systems. For most of the TEM measurement a 200 m × 200 m square source loop was used and in some difficult terrain a 100 m × 100 m square. With Zonge TEM the measurements were made at the frequencies 32, 16, 8 and 4 Hz, and with Phoenix equipment at 25, 5 and 1 Hz.

To read and process the TEM data, a software called TemX was used (Árnason, 2006a). The TemX programme reads TEM raw data files acquired by the PROTEM digital receiver of Zonge. The programme calculates average and standard deviations of repeated transient voltage measurements and calculates late time apparent resistivity as a function of time. The program has a graphical interface, offering the possibility of editing or omitting outliers of noisy raw data. In this project the raw data from Zonge were processed by using the software temxUSF.

The TEMTD programme for the inversion process assumes that the source loop is a square loop and that the receiver coil/loop is at the centre of the source loop (Árnason, 2006b). The current wave form is assumed to be a half-duty bipolar semi-square wave with exponential current turn-on and linear current turn-off. The program is written in ANSI-C and runs under UNIX/LINUX operating systems. It uses the gnuplot graphics program for graphical display during the inversion process.

The inversion algorithm used in the programme is the Levenberg-Marquardt non-linear least square inversion as described by Árnason (1989). The misfit function is the root-mean-square difference between measured and calculated values (chi-square), weighted by the standard deviation of the

measured values. The user can choose whether the program fits the measured voltage values or the late time apparent resistivity values.

The programme offers the possibility to keep models smooth, both with respect to resistivity variation between layers (actually logarithm of conductivities) and layers thicknesses (actually logarithm of ratio of depth to top and bottom of layers). The program can be used to perform minimum structure (Occam) inversion. The input file for TEMTD is the *.inv file produced by the TemX program.

All the TEM sounding were 1D inverted using TEMTD and Occam inversion. An example is given in Figure 10. The TEM and magnetotellurics data from the Alallobeda geothermal prospect and the results of the processing are published in a separate appendices report (Hailegiorgis, G., 2015). All the TEM soundings curves and the associated 1D models are presented in Appendix I. An initial model is given and the best fitting model based on a layered model followed by running TEMTD. The output from the layered model is used as an initial model in the Occam inversion. To get a smooth model and good fit, several parameters can be changed.

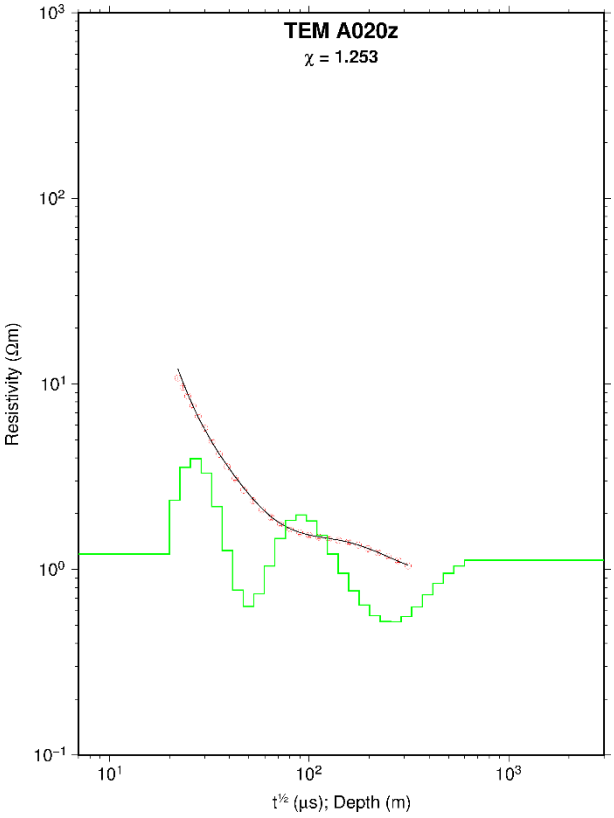

FIGURE 10: A typical TEM sounding from Alallobeda prospect and its 1D Occam inversion; red circles: measured late-time apparent resistivity; black line: apparent resistivity calculated from the model shown in green. The number on the top of the figure (A020z) corresponds to the name of the station

6.3 MT data processing and inversion

MT data were collected using a 5-channel MTU unit data acquisition system from Phoenix Geophysics Company Canada. In this project work 54 soundings were processed from the time series data and used for interpretation.

The time series data were downloaded from the compact flash card of MTU-5A units and viewed using the Synchro Time Series View program. This program allows imaging and printing of graphical representations of the raw time-series data, it computes power spectra densities derived from the time-series data and coherence between pairs of orthogonal channels. The SSMT2000 program, which is provided by Phoenix Geophysics in Canada (Phoenix Geophysics, 2005), takes as input raw time series files, calibration files and site parameter files. In an intermediate step, it produces Fourier coefficients which are then reprocessed with data from reference sites, using robust routines. The output are MT plot files (MTH and MTL) containing multiple cross powers for each of the frequencies. The program MTeditor takes the output from the SSMT2000 program and displays resistivity and phase curves as well as the individual cross powers that are used to calculate each point on the curve. Cross powers that were affected by noise can be automatically or manually excluded from the calculation. When the final cross power and auto-powers as well as all relevant MT parameters have been calculated, the files are converted and stored to industry-standard EDI (Electronic Data Interchange) files suitable for use with Geophysical interpretation software like TEMTD where a joint inversion with TEM data from the same site is carried out. In this project work, EDI files were processed and inverted with the program TEMTD (similar as inversion with the TEM data, as mentioned in Section 6.1). In the project, the rotationally invariant apparent resistivity and phase calculated from the determinant of the impedance were jointly

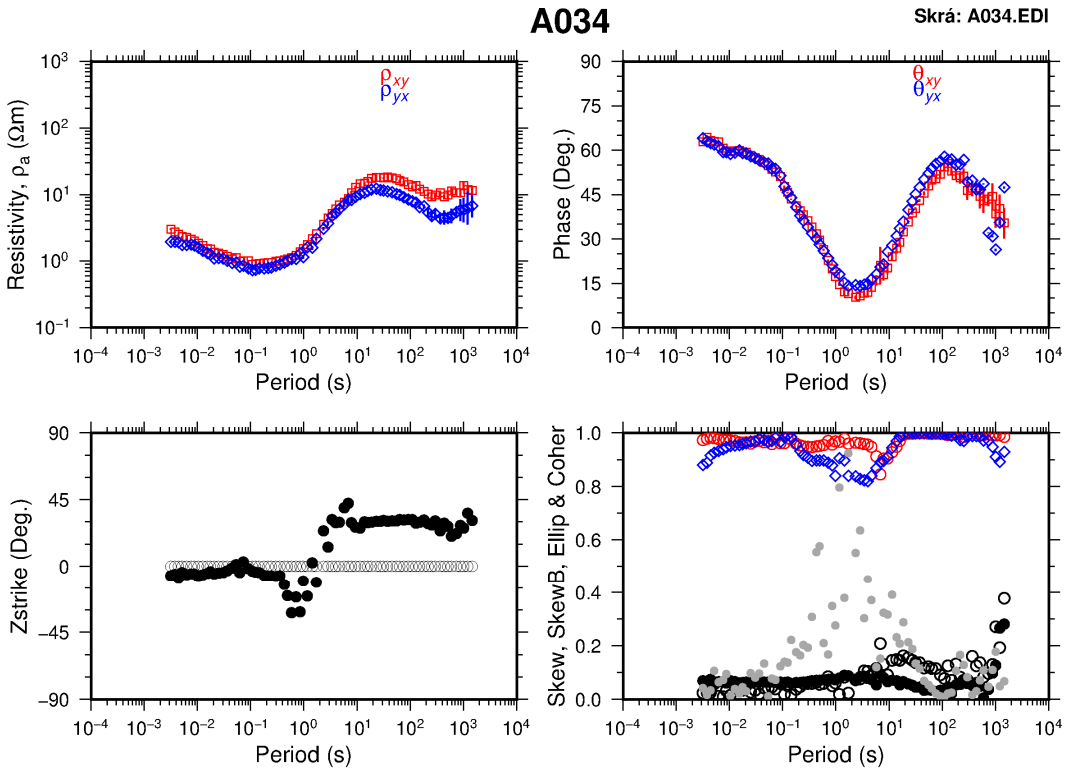

FIGURE 11: An example of processed MT data from the Alallobeda prospect area. The plots show the apparent resistivity and phase derived from the xy (red) and yx (blue) components of the impedance tensor, the Z-strike or Swift angle (black dots), multiple coherency of xy (red) and yx (blue), skew (black dots) and ellipticity (gray dots)

inverted with the TEM data using Occam inversion. The TEMTD programme determines the best static shift parameters for MT data.

The EDI files were converted from DOS to Unix format. The script spect2edi is used to transform the data into EDI form and then the edi2ps script is used to produce PostScript plots of all relevant available parameters of the EDI file. Ghost view (gv) is used to view the apparent resistivity, phase, Zstrike, Tstrike etc. An example of the processed MT data is given in Figure 11. The processed data of all the MT soundings are shown in Appendix II (Hailegiorgis, G., 2015).

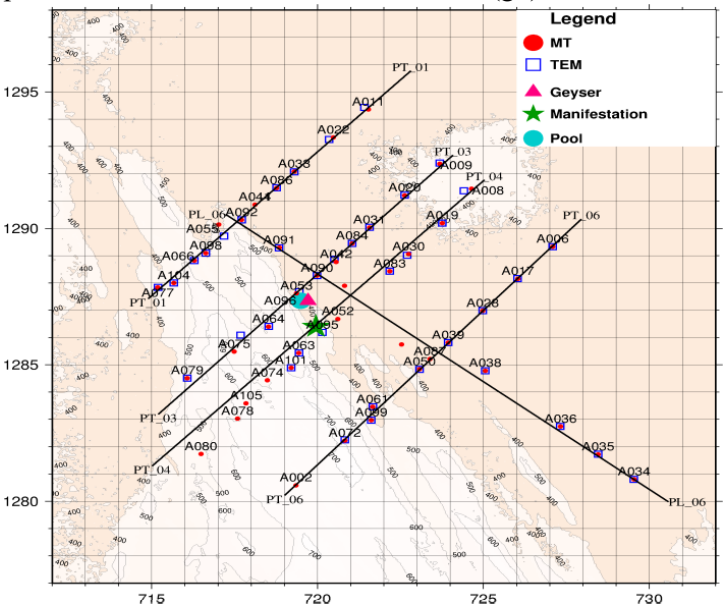

FIGURE 12: Location map of TEM and MT soundings

At some of MT stations, the TEM data from the same site which was acquired using the Phoenix instrument could not be used. Those were inverted by fixing the static shift value by running the script for MT only. For these stations the static shift was given by the ELC-Consult.

Figure 12 shows the location of TEM and MT soundings, the black lines show the profiles that were used for cross-sections.

6.4 Static shift correction

Static shift occurs because of near surface resistivity inhomogeneities and topographic effects. It is due to electric field distortion because of the dependency of electric field on the resistivity of the material where the voltage difference is measured. Static shift due to the topographic effect results in current distortion. The induced current density which is mostly flowing laterally is spread out in local topographic highs but concentrated in topographic lows. So the apparent resistivity value on topographic highs is low and vise versa. Furthermore, MT suffers from static shift problems. Unlike the electric field, the magnetic field is relatively unaffected by local or near surface inhomogeneities. Therefore, static shift due to near- or sub-surface inhomogeneities and topographic effects can lead to severe problems in the interpretation of MT data. The apparent resistivity curve is shifted upward due to low-resistivity slab and shifted downward due to high resistivity when it is plotted on log scale. This shifting gives a wrong resistivity model. Figure 13 shows the histogram of the static shift parameters and reveals how the apparent resistivity curve of the MT data is shifted upwards or downwards. The multiplier for all 54 MT soundings is given, with all except one found to be in the range of 0.2-1.6.

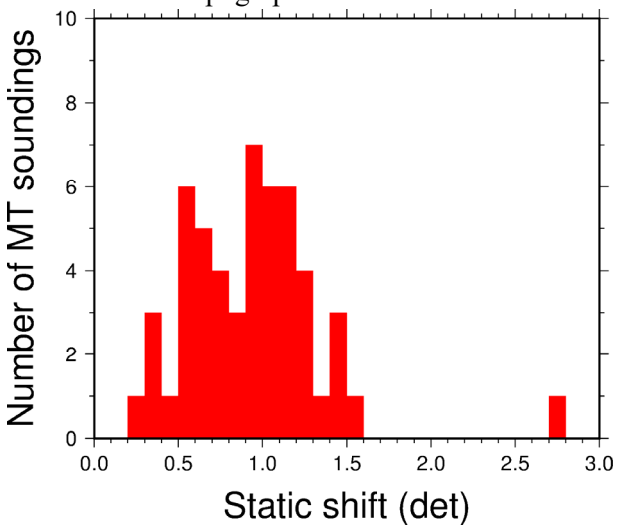

FIGURE 13: A histogram of static shift parameters for Alallobeda prospect

Static shift is frequency independent and is not visible in the phase. Static shift causes a frequency independent offset in apparent resistivity curves so that they are plotted parallel to their true level but scaled by a factor. These static shift factors cannot be determined directly from MT data recorded at one single site. A parallel shift between two polarizations of apparent resistivity curves is a reliable indicator that static shift is present in the data. However, lack of shift between two apparent resistivity curves does not necessarily guarantee an absence of static shift, since both curves might be shifted by the same value. The correct level of the apparent resistivity curves may lie above, below or between the measured levels. If MT data are interpreted applying 1D modelling without correcting for static shift, the depth to the conductive body will be shifted by the square root of the factor by which the apparent resistivities are shifted ($\sqrt{s}$) and the modelled resistivity will be shifted by s. 2D and 3D models may contain extraneous structure if static shift is ignored. Figure 14 shows the spatial distribution of static shift multipliers in the Alallobeda prospect. In most of the area, the MT apparent resistivity is shifted downwards, but upwards at its border.

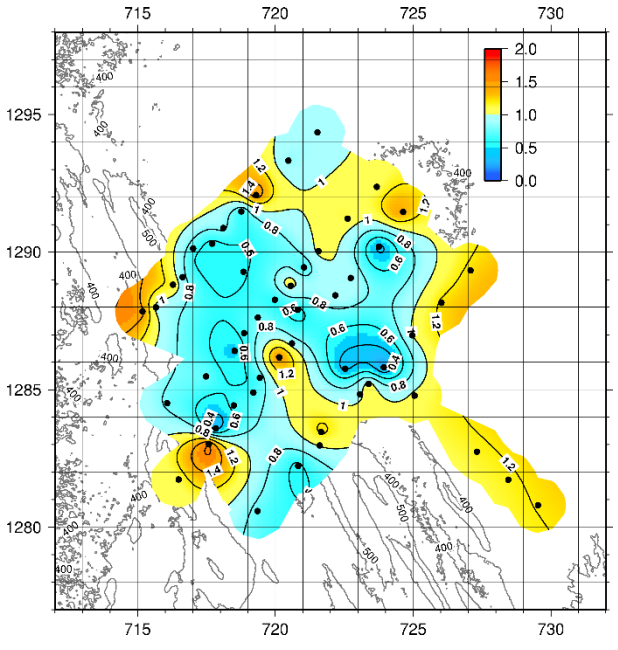

FIGURE 14: Spatial distribution of static shift parameters in the Alallobeda prospect

Static shift can be corrected by short period corrections relying on active near-surface measurements like TEM. TEM does not have the static shift problems that affect MT soundings. Because TEM does not use electrodes and because it does not require electrical contact with the earth for data acquisitions and magnetic field

is not much affected by static shift problems except at very high frequencies (Groom and Bailey, 1989) while the electric field can be severely affected. The static shift problem occurs because the electromagnetic field is distorted by shallow resistivity anomalies near the MT station or close to the electrodes or by the topographic effect. TEM can be used in conjunction with MT data from the same site to correct static shift in MT data. Apparent resistivity curves derived from MT data can be scaled so that they tie-in with TEM curves or can be jointly inverted with TEM data (Sternberg et al., 1988). These techniques are only effective for correcting static shift arising from near-surface inheterogeneities. If the impedance phases are split at high frequencies which are expected to have similar penetration depth for TEM data, then there is no justification for supposing that the apparent resistivity curves for the two polarizations should lie at the same level.

6.5 Joint 1D Occam inversion of TEM and MT soundings

The inversion programme TEMTD (Árnason, 2006b) was used to perform joint 1D Occam inversion of TEM and MT data using the apparent resistivity and phase derived from the rotationally invariant determinant of the impedance tensor. The programme determines the best static shift parameter for the MT data.

Figure 15 shows an example of a joint 1D Occam inversion of TEM and MT data. A complete set of all the 1D joint inversion results is shown in Appendix III (Hailegiorgis, G., 2015). On the right side is shown the response of the resistivity model with depth. The red curve shows the measured value of the TEM sounding, the dark blue line shows measured values of the MT sounding, while in light blue deleted point are marked. Also shown are the values of chi and static shift.

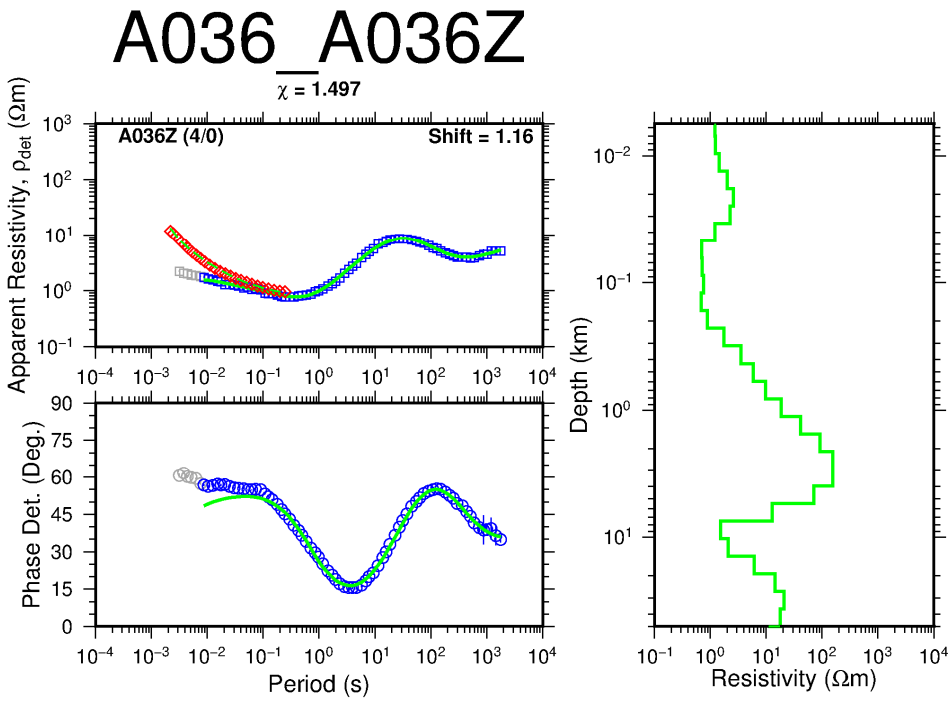

FIGURE 15: Joint 1D inversion of MT and TEM soundings with TEM apparent resistivities transformed to a pseudo-MT curve; blue circles: apparent phase derived from the determinant of MT impedance tensor; light blue symbols to the left of the green curve: data not used in the inversion; vertical blue lines: error bars. Green lines show the response of the model calculation. On the right are shown results of the 1D resistivity inversion model, while on the left its synthetic MT apparent resistivity and phase response. Number on the top of the Figure: A036 is name of the MT station and A036Z is the name of the TEM station. The numbers in parenthesis (4/0) indicates that the two stations were 4 m apart and their elevation difference was 0 m. Static shift correction was 1.16

7. RESULTS AND DISCUSSION OF MT AND TEM SURVEY

7.1 Resistivity cross-sections

The programme TEMCROSS, which was developed at ÍSOR (Eysteinsson, 1998), was used to create the resistivity cross-sections based on the joint 1D Occam inversion models of the TEM and MT data shown in Appendix III (Hailegiorgis, G., 2015). The cross-sections are plotted to a depth of 10,000 m and some also only down to 2,000 m. Their locations are given in Figure 12. Four cross-sections run perpendicular to the tectonic structure (PT_01, 03, 04, and 06) and one parallel to it (PL_06). Additional cross-sections are given in Appendix IV (Hailegiorgis, G., 2015). Generally, it can be said that the resistivity structure seen in the cross-sections is quite similar, with three main resistivity layers. At the top is a fairly thin (few hundred metres) low-resistivity layer (< 10 Ωm) which can be correlated to shallow sedimentary formations. Below that, there is usually a thick high-resistivity formation (> 100 Ωm), which correlates with the highly resistive Afar Stratoid series basalt. At the bottom the resistivity is again low, usually < 10 Ωm, which may indicate a deeper lying conductor that could be related to the heat source. In more detail, the following can be said:

Resistivity cross-section PL_06 is shown in Figure 16 down to a depth of 10,000 m but in Figure 17 only down to 2,000 m. It runs NW-SE parallel with the main geological structure and crosses the main

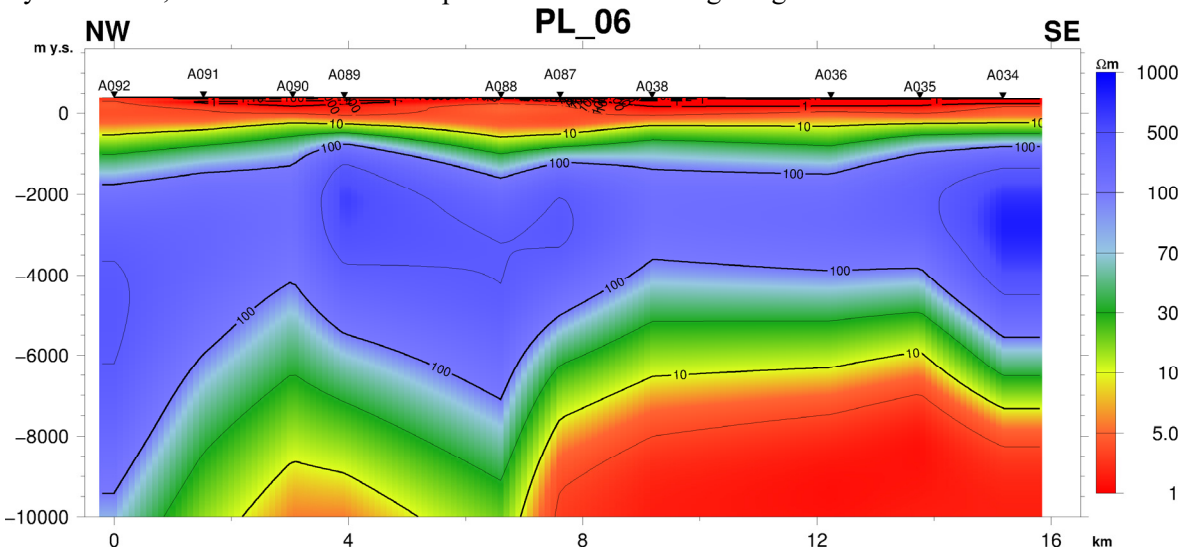

FIGURE 16: Resistivity cross-section PL_06 down to 10,000 m b.s.l.; for location see Figure 12

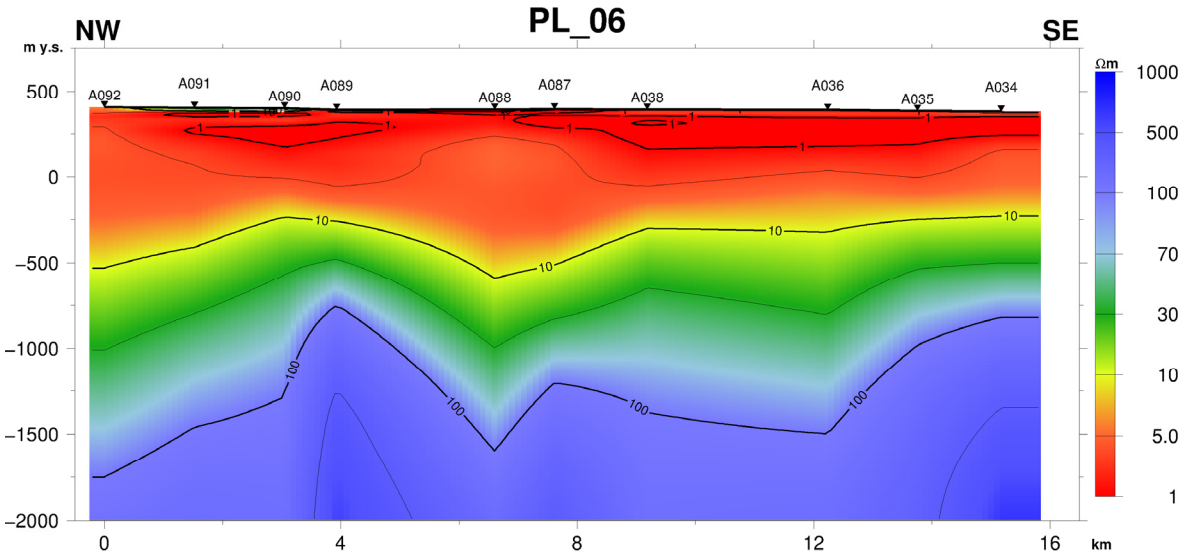

FIGURE 17: Resistivity cross-section PL_06 down to 2,000 m b.s.l.

area of surface manifestations. Down to a depth of 300 m b.s.l., the cross-section is characterized by a thin layer of very low resistivity (< 10 Ωm) correlated to the shallow sedimentary formation. Below that the resistivity increases considerably, with this layer showing resistivity values > 100 Ωm, reaching down to a depth of 4000-6000 m b.s.l., corresponding with the highly resistive Afar Stratoid series basalt, but high-temperature alteration minerals chlorite and epidote may also contribute here. At greater depth the resistivity decreases to a value of < 10 Ωm which may indicate the deeper lying conductor.

Resistivity cross-section PT_01 is shown in Figure 18, down to a depth of 10,000 m. It runs from SW-NE, perpendicular to the main geological structures. The cross-section is characterized by the low-resistivity anomaly, < 10 Ωm, down to a depth of approx. 300 m b.s.l., associated with the shallow sedimentary formation. Around station A086 an upflow zone is seen. Below the low resistivity the high-resistivity layer is found with resistivity values around 100 Ωm down to depths varying between 1000 and 5000 m from the surface. This high resistivity is believed to be mainly related to the highly resistive Afar Stratoid basalt series. At greater depth the resistivity decreases to a value of < 10 Ωm, indicating the deeper lying conductor that may be related to the heat source. This low-resistivity body is seen both in the southwest and northeast part of the cross-section, while between stations A066 and A033 the resistivity is high, around 100 Ωm.

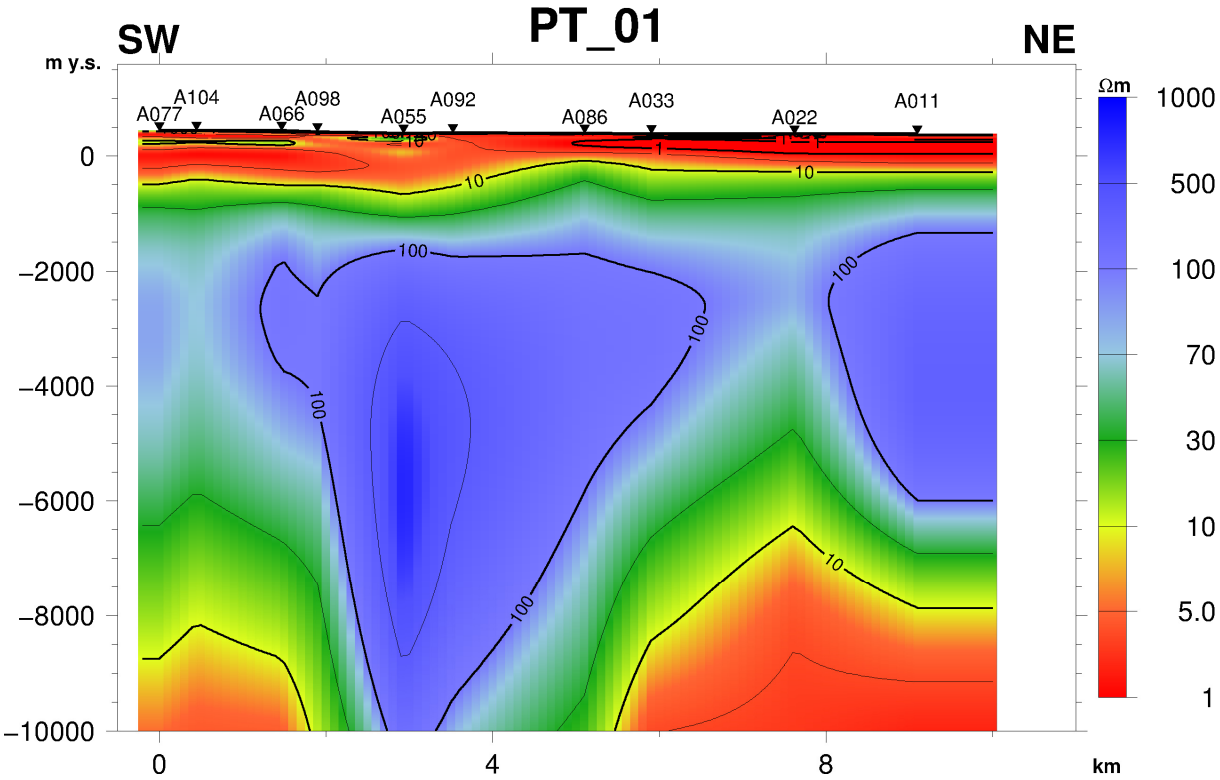

FIGURE 18: Resistivity cross-section PT_01, down to 10,000 m b.s.l.; for location see Figure 12

Resistivity cross-section PT_03 is shown in Figure 19 and runs NE-SW perpendicular to the geological structure. The uppermost part of the cross-section is characterized by a thin layer of very low resistivity, < 10 Ωm, down to a depth of 200 m b.s.l. Below stations A053 and A079 the resistivity is slightly higher, with a value of 10 Ωm, indicating unaltered lava. This low-resistivity layer is associated with the sedimentary formation and possibly also influenced by low-temperature alteration minerals like smectite and zeolites. Below the low-resistivity top layer there is a high-resistivity body with resistivity values about 100 Ωm reaching from approx. 700 m down to the depth 5000 m b.s.l., correlating to the Afar Stratoid basalt series possibly with some influence from high-temperature alteration minerals like chlorite and epidote. This high-resistivity layer is mainly seen in the southwest part of the profile, while in the northeast part a low-resistivity anomaly is dominant. Like in the other cross-sections, at greater

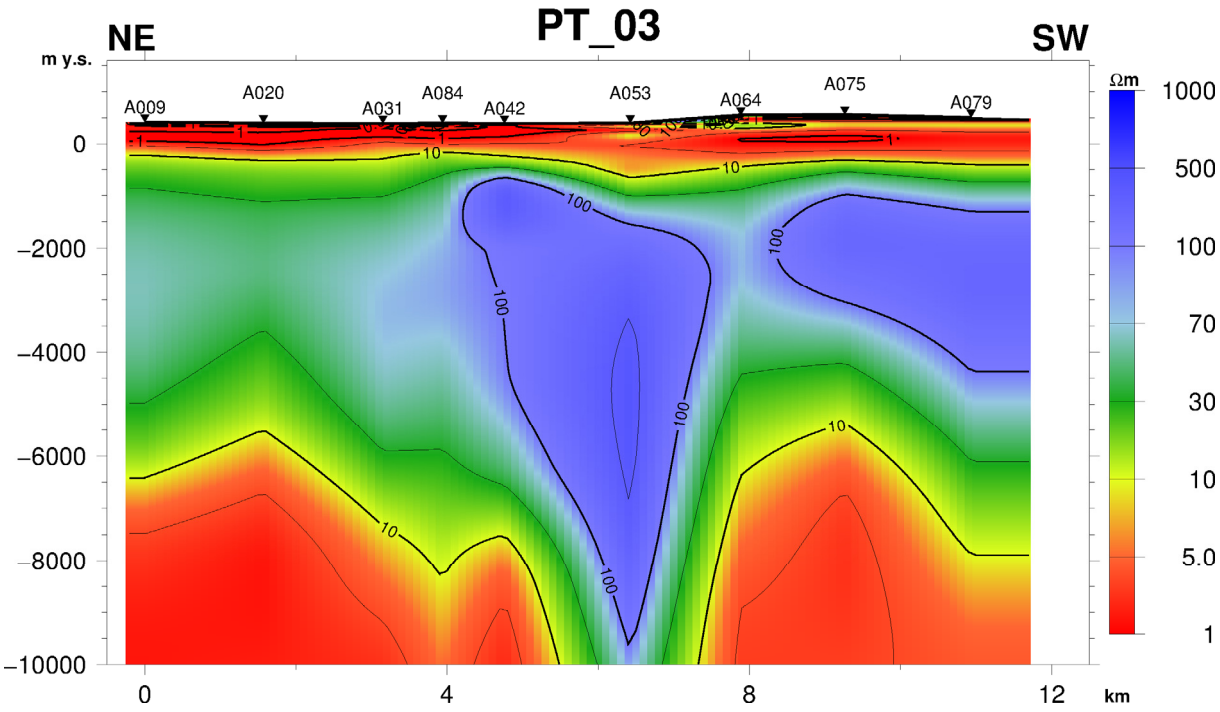

FIGURE 19: Resistivity cross-section PT_03, down to 10,000 m b.s.l.

depth the resistivity decreases to a value of < 10 Ωm. This low-resistivity layer is seen both in the northeast and southwest part of the profile, while between stations A084 and A053 the deep resistivity is high with a value of 100 Ωm seen to the bottom of the cross-section.

Resistivity cross-section PT_04 is shown in Figure 20 down to 10,000 m b.s.l. and in Figure 21 down to 2000 m b.s.l. It runs NE-SW, perpendicular to the geological structures. The uppermost part of the cross-section is characterized by a thin layer of very low resistivity (< 10 Ωm) down to a depth of 400 m b.s.l., associated with the sedimentary formations. Below, the high-resistivity layer with resistivity values between 100 and 1000 Ωm is seen, reaching down to depths of 1000-5000 m b.s.l. The resistivity

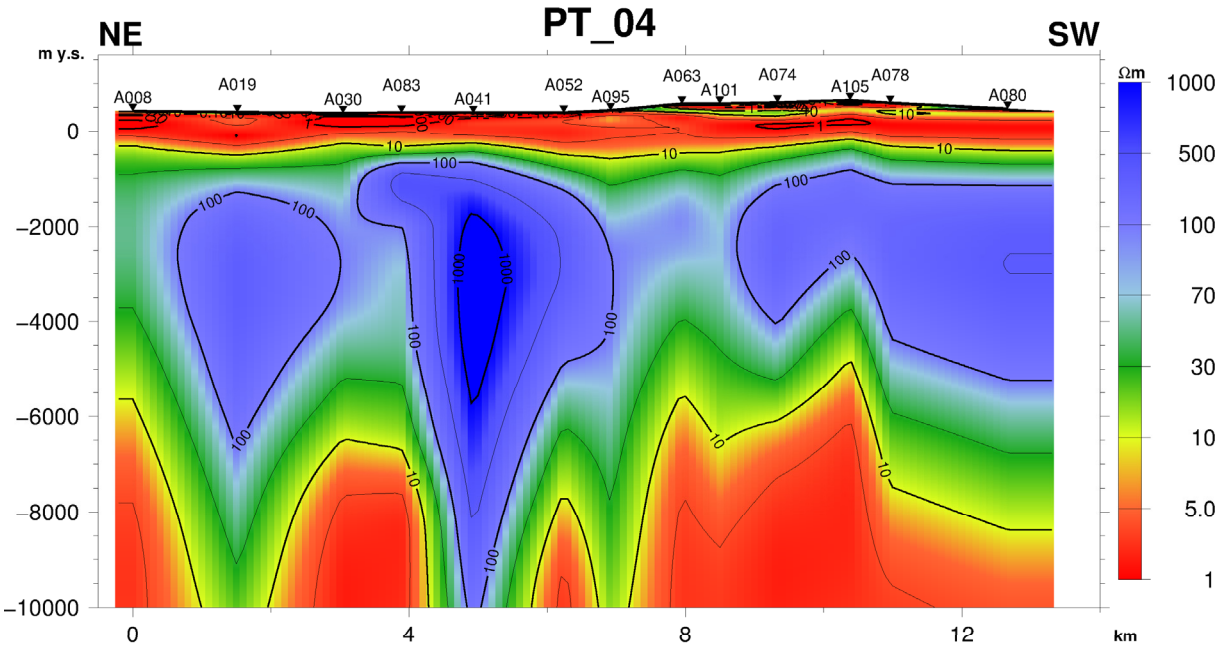

FIGURE 20: Resistivity cross-section PT_04, down to 10,000 m b.s.l.

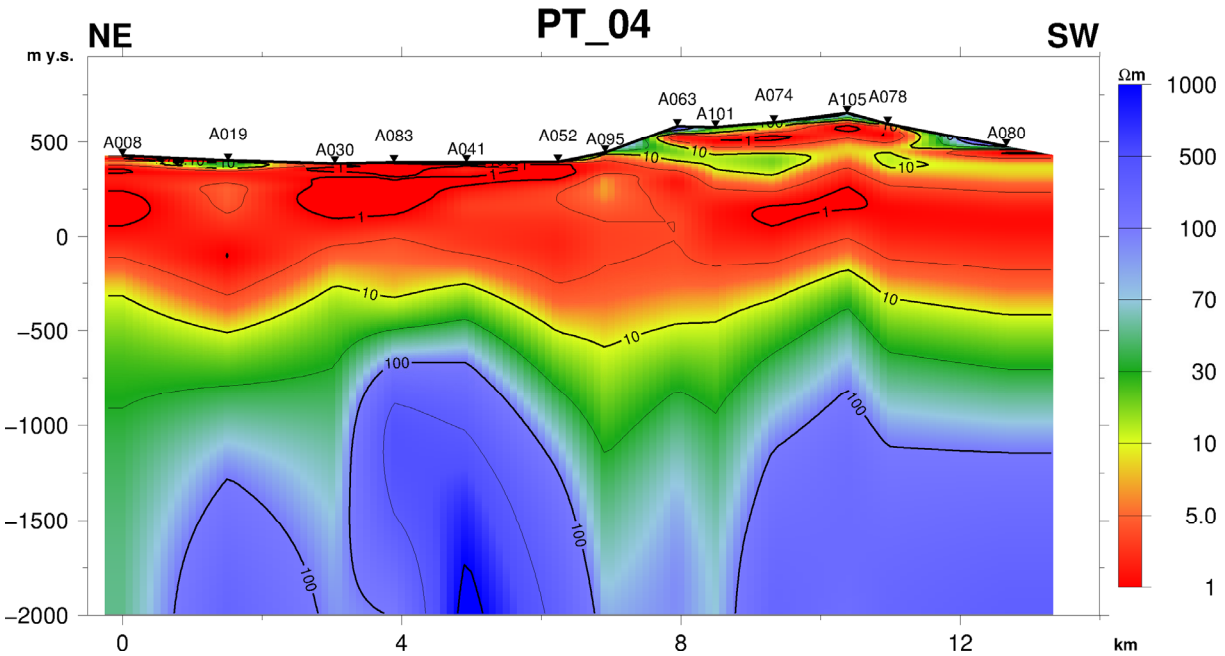

FIGURE 21: Resistivity cross-section PT_04, down to 2,000 m b.s.l.

structure around stations A041, A083 and A105 may indicate an upflow zone in that area. As before, the high resistivity is believed to correlate to the Afar Stratoid basalt series, possibly also influenced by high-temperature alteration minerals like chlorite and epidote. At greater depth the resistivity decreases again, reaching quite low values, < 10 Ωm which may indicate the deeper lying conductor, related to the heat source. This low-resistivity zone is found below all stations except station A041 which shows very high resistivity down to great depth.

Resistivity cross-section PT_06 is shown in Figure 22. It runs NE-SW, perpendicular to the main geological structures. The shallow part of the cross-section is characterized by the thin low-resistivity layer, with a resistivity of 1 Ωm, reaching down to a depth of 200 m b.s.l., associated with the shallow sedimentary formations and low-alteration minerals like smectite and zeolite. Below the low-resistivity

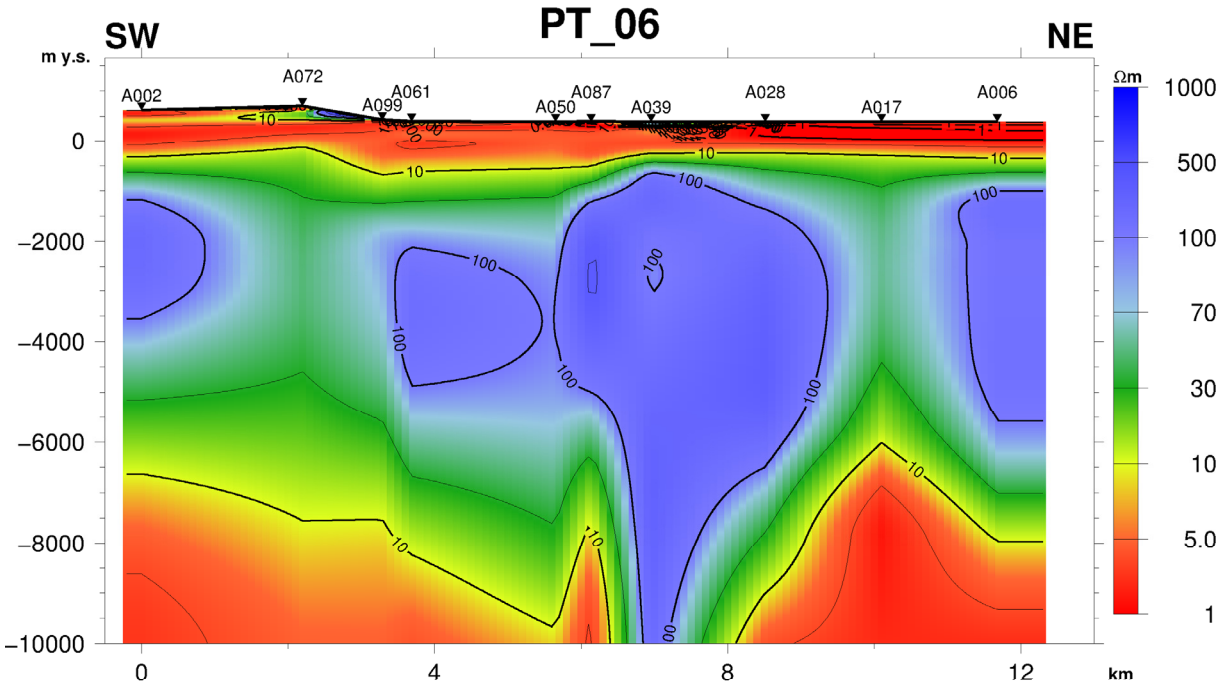

FIGURE 22: Resistivity cross-section PT_06, down to 10,000 m b.s.l.

top, there is high-resistivity layer, the resistivity increases to a value of around 100 Ωm, reaching down to a depth of at least 4,000 m b.s.l., reflecting the Afar Stratoid basalt series. At greater depth the resistivity decreases again, to values of < 10 Ωm, as in other cross-sections, probably indicating a deeper lying conductor possibly related to heat source. This low-resistivity zone is seen both in the southwest and northeast parts of the cross-section. Below station A039 the high resistivity reaches greater depths, separating the deep low-resistivity conductors.

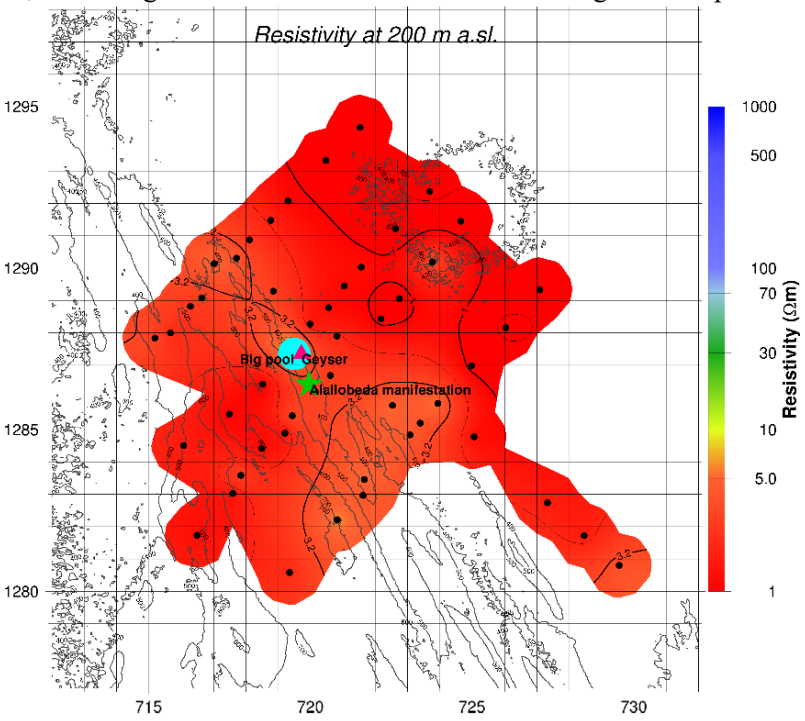

FIGURE 23: Iso-resistivity map of Alallobeda prospect at 200 m a.s.l.; the black dots indicate locations of MT soundings, light blue filled circle the big geothermal pool, with the pink triangle denoting the Geysers; and the green star indicates surface manifestations

7.2 Iso-depth resistivity maps

The programme TEMRESD developed at ÍSOR (Eysteinsson, 1998) was used to plot the iso-resistivity maps based on the joint 1D Occam inversion models of the TEM and MT data presented in Appendix III (Hailegiorgis, G., 2015). The programme runs in Linux environment. The elevation of the Alallobeda geothermal field varies from 200 to 800 m a.s.l. The iso-resistivity maps are presented from 200 m a.s.l. to 8000 m b.s.l. Here 4 maps are shown with additional maps given in Appendix IV (Hailegiorgis, G., 2015).

Resistivity map at 200 m a.s.l. is shown in Figure 23. The resistivity is very low (< 10 Ωm) for the whole area and reflects the sedimentary formation found at shallow levels in the area and low-temperature alteration minerals like smectite and zeolites.

Resistivity map at 300 m b.s.l. is presented in Figure 24. The higher resistivities associated with the Afar Stratoid basalt series are influencing the map, with resistivities around 30 Ωm seen at this depth level. A structure of relatively low

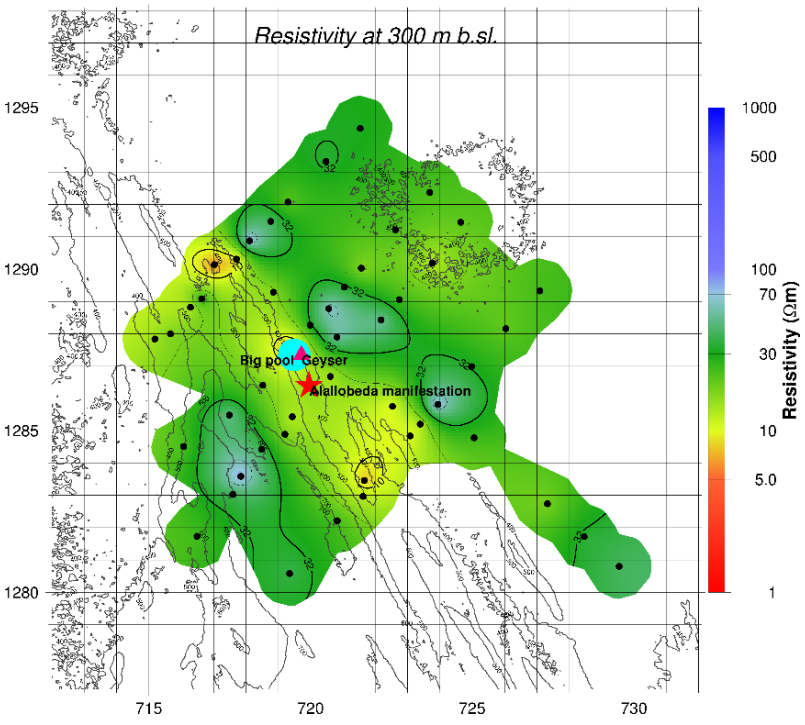

FIGURE 24: Iso-resistivity map in Alallobeda prospect at 300 m b.s.l.; for figure legend see Figure 23

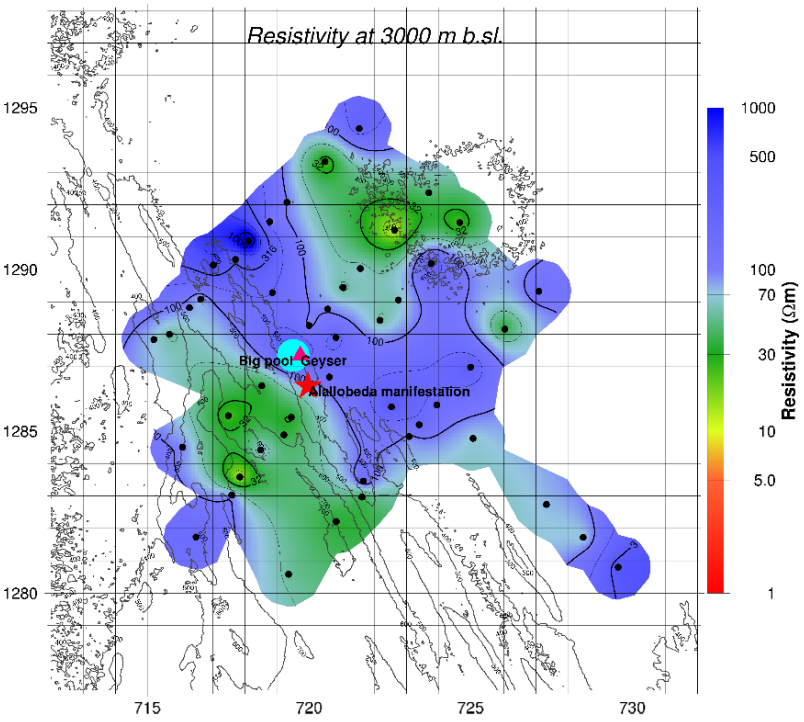

FIGURE 25: Iso-resistivity map in Alallobeda prospect at 3000 m b.s.l.; for figure legend see Figure 23

resistivity is seen along the geological NW-SE structure. This might be correlated with lateral flow of geothermal fluids, fractures or low-temperature alteration minerals like smectite and zeolite.

Resistivity map at 3000 m b.s.l. is shown in Figure 25. The resistive layer correlated with the Afar Stratoid basalt series is seen in the whole area with the resistivity showing values above 100 Ωm. However, along the geological structures trending NW-SE the resistivity is still fairly low at this depth, indicating lateral flow of geothermal fluids along the main fractures, and low-temperature alteration minerals like smectite and zeolites.

Resistivity map at 8000 m b.s.l. is shown in Figure 26. Here the deep lying low-resistivity zone is clearly manifested, with an average resistivity of approximately 3.2 Ωm. This explanation for this deep lying conductor is not certain, but it may be related to the heat source or deep saline sediments. Interestingly, a resistivity anomaly can be seen along the main geological structure trending NW-SE, including the big pool, with slightly resistivities (10 Ωm), supporting geothermal activity along this structure.

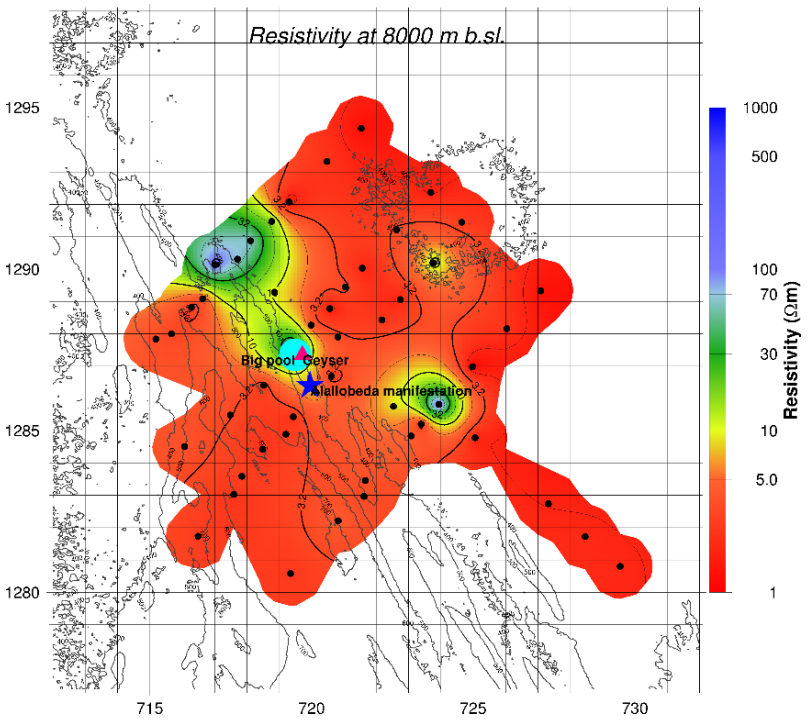

FIGURE 26: Iso-resistivity map in Alallobeda prospect at 8000 m b.s.l.; for figure legend see Figure 23

8. STRIKE ANALYSIS

Strike directions give information on the dimensionality of rock formation and the direction of the main resistivity contrast. Here it is not important if the resistivity distribution is 2D or 3D. This can be shown through the Zstrike which is based on H_x and H_y (see 5.1.2) and through induction arrows which are calculated from H_z. Two maps are presented here with additional maps given in Appendix V (Hailegiorgis, G., 2015). Figure 27 shows the Zstrike calculated from H_x and H_y at 0.01-0.1 s corresponding to a shallow depth of some hundreds of m. The strike is parallel to the main resistivity contrast and coincides with the geological strike direction in the Alallobeda geothermal field.

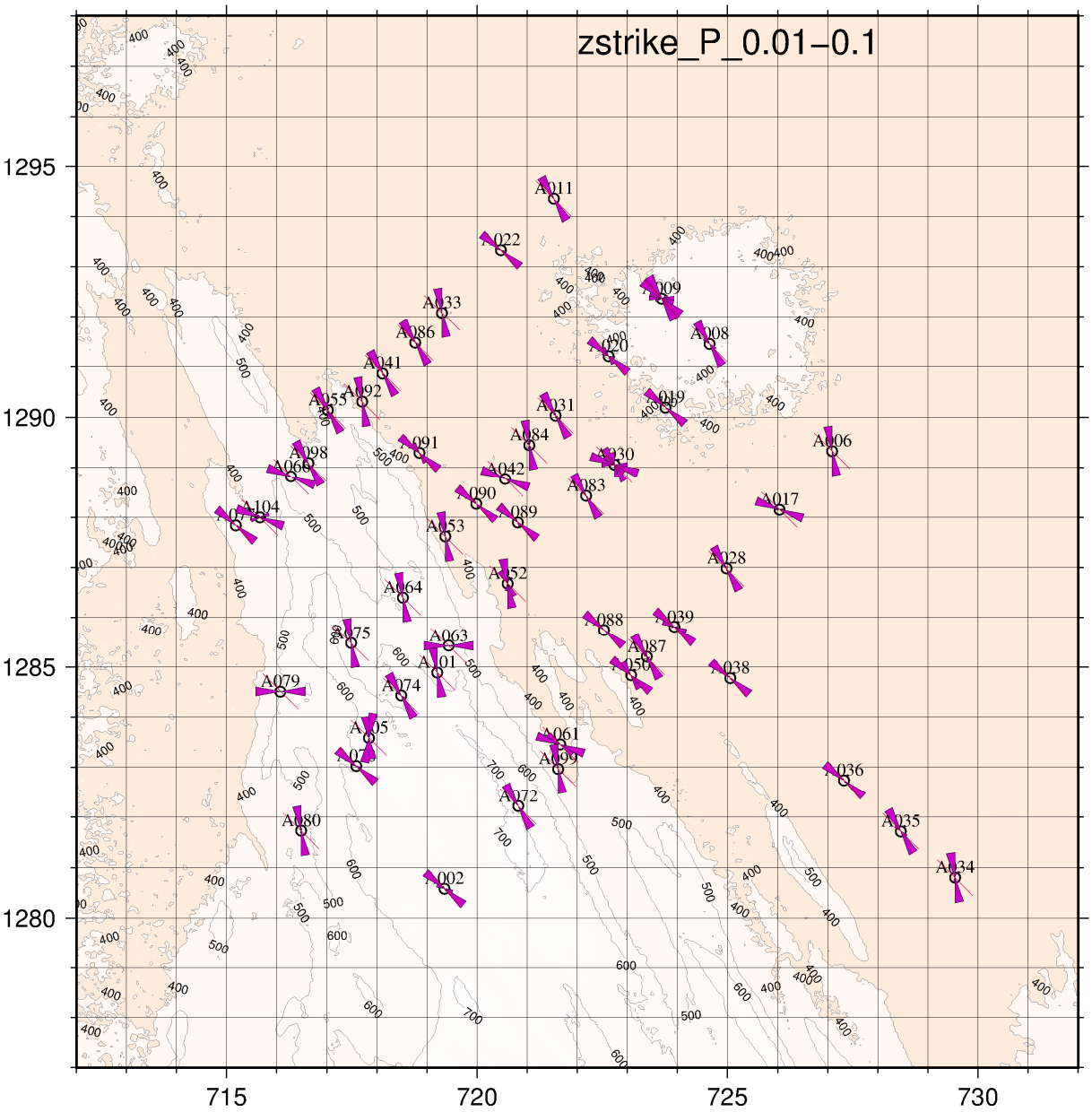

FIGURE 27: Rose diagram of the electrical strike direction based on the Zstrike calculated from H_x and H_y at 0.01-0.1 s corresponding to a shallow depth of some hundreds of metres. The strike is parallel to the main resistivity contrast and coincides with the geological strike direction

Figure 28 shows the anomaly directions for induction arrows. The The real induction arrows (blue colour) point away from a zone of low resistivity. The induction arrows are consistent with the resistivity contrast.

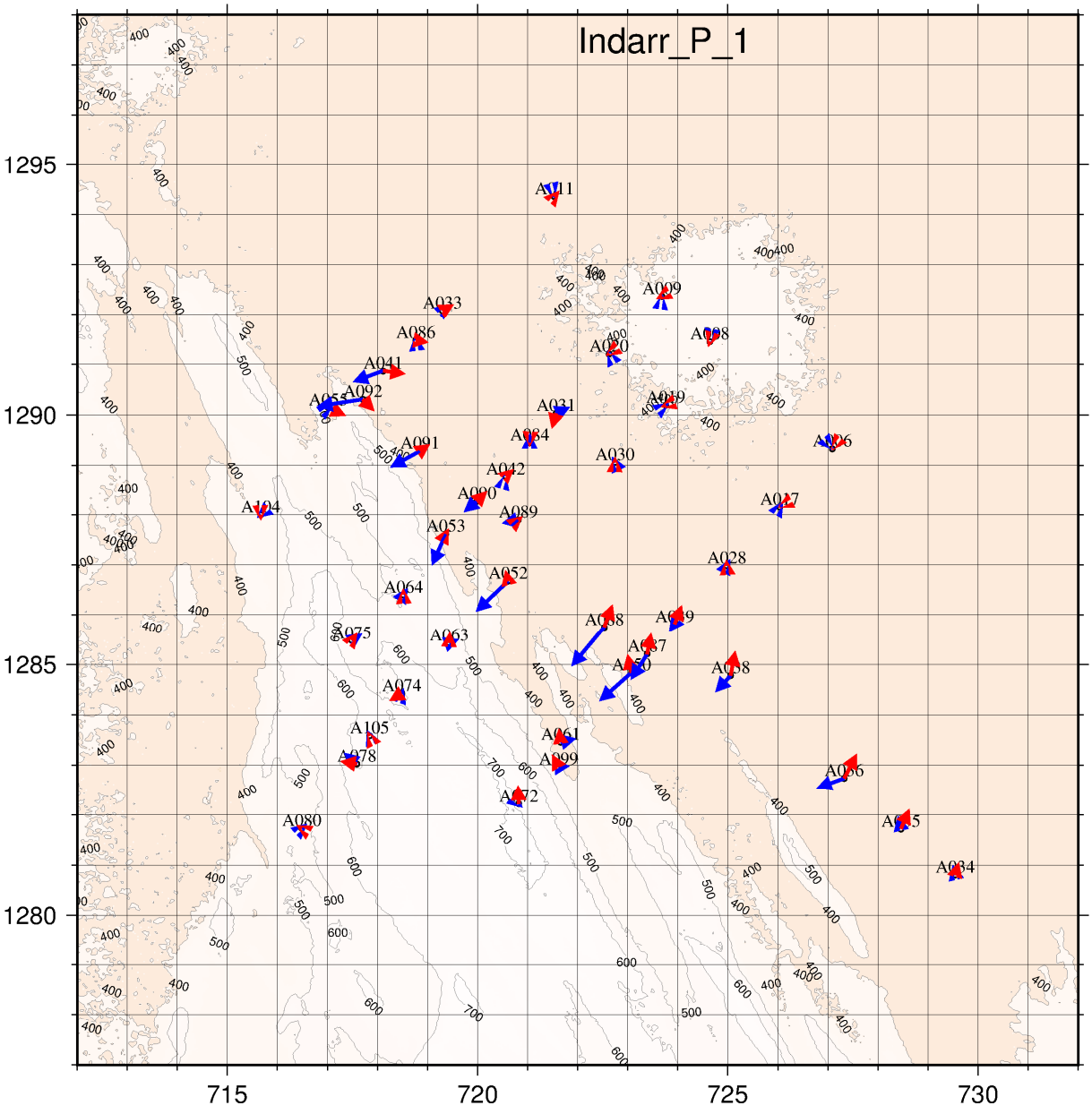

FIGURE 28: Induction arrows for the period 1 s, corresponding to a depth of a few km; blue arrows denote the real part and red arrows the imaginary part

9. CONCLUSIONS

Based on the result of the joint 1D inversion of 54 MT and TEM soundings, the resistivity structure reveals three main resistivity layers seen in the cross-sections presented:

- At shallow depths down to about 500 m b.s.l., a thin layer of low resistivity values exists (< 10 Ωm), which can be correlated to the shallow sedimentary formations in the area, with some influence noted from lateral flow of geothermal fluid in fractures.
- Below the sediments, the resistivity increases considerably and reaches values of about 100 Ωm at a depth of 1000 m b.s.l. This layer is associated with the low-permeability Afar Stratoid basalt series. As can be seen from the cross-sections, this layer stretches to deep levels often of the order of 5-6000 m b.s.l.
- Below the high-resistivity layer, another low-resistivity layer is seen (< 5 Ωm). This deep conductor is either related to the heat source or highly saline sediments at deep levels.
- Effect of geothermal upflow is seen in the iso-resistivity maps associated with known geothermal structures.
- Results of the strike analysis are in an agreement with the resistivity model.

ACKNOWLEDGEMENTS

It has been a great pleasure to participate in this training. I would like to express my special gratitude towards the UNU-GTP director Mr. Lúdvík S. Georgsson, and his deputy Mr. Ingimar G. Haraldsson for the opportunity to participate in the 6-month geothermal training programme in Iceland. I am highly indebted to the UNU-GTP staff members Ms. Málfrídur Ómarsdóttir, Ms. Thórhildur Ísberg and Mr. Markús A.G. Wilde for their guidance and help. I wish to give my thanks to all lecturers and staff members of ÍSOR for their comprehensive presentations and willingness to share their knowledge and experience.

I would like to express my sincere gratitude to my advisors Gylfi Páll Hersir and Knútur Árnason for continued support for my project, for their patient, motivation and immense knowledge. You have set an example of excellence as advisor, instructor and role model.

I would like to express my special gratitude and thanks to ICEDA people for giving me the opportunity to use the data for my project. I am highly indebted to ELC-Consult Company people for providing all the necessary information and data regarding my project and also for their support in completing my project.

I would like to offer my special thanks to Ato Hunda Meleka chief geologist of Geological Survey of Ethiopia, Ato Solomon Kebede Geothermal Resource Exploration and Evaluation Assessment directorate, granting me permission to attend this training and for their continued support, help and encouragement. I express my deep sense of gratitude to Mr. Yiheyis Kebede and all my colleagues in the geothermal department back home giving all necessary information for my project and people who have willingly helped me out with their abilities.

I would like to express my deepest appreciation to my devoted family and friends for their love, prayers, encouragement and motivation.

I would like to thank all 2015 UNU fellows for making my stay in Iceland more pleasurable. Special thanks to my geophysicist UNU Fellows Amali, Ali and Lee and also Fredrick for sharing their experiences and knowledge. Special thanks to Nyaso and Hamda for the good time we spent together.

I would like to thank the Almighty God who helped me all the way. May he bless all of you.

REFERENCES

Acocella, V., Abebe, B., Korme, T., and Barberi, F., 2008: Structure of Tendaho Graben and Manda Hararo rift: implications for evolution of the southern Red Sea propagator in central Afar. *Tectonics, 27,* 17 pp.

Aquater, 1980: *Geothermal resource exploration project Tendaho area, feasibility study - Phase II.* EIGS and Ministry of Foreign Affairs of Italy, San Lorenzo in Campo, report.

Aquater, 1995: *Micro seismic study, final report.* EIGS and Ministry of Foreign Affairs of Italy, San Lorenzo in Campo, report.

Aquater 1996: *Tendaho geothermal project, final report.* MME, EIGS - Government of Italy, Ministry of Foreign Affairs, San Lorenzo in Campo, report.

Archie, R.G., 1942: The electrical resistivity log as an aid in determining some reservoir characteristics. *Trans. AIME, 146,* 54-67.

Árnason, K., 1984: The effect of finite electrode separation on Schlumberger soundings. *54th Annual International SEG Meeting, Atlanta, Expanded Abstracts,* 129-132.

Árnason, K., 1989: *Central loop transient electromagnetic sounding over a horizontally layered earth*. Orkustofnun, Reykjavík, report OS-89032/JHD-06, 129 pp.

Árnason, K., Karlsdóttir, R., Eysteinsson, H., Flóvenz, Ó.G., and Gudlaugsson, S.Th., 2000: The resistivity structure of high-temperature geothermal systems in Iceland. *Proceedings of the World Geothermal Congress 2000*, *Kyushu-Tohoku, Japan,* 923-928.

Árnason, K., 2006a: *TemX, short manual.* ISOR, Reykjavík, internal report, 17 pp.

Árnason, K., 2006b: *TEMTD (Program for 1D inversion of central-loop TEM and MT data)*. ISOR, Reykjavík, short manual 16 pp.

Barberi F., Ferrara G., Santacroce R., and Varet J., 1975: Structural evolution of the Afar triple junction. In: Pilger, A., and Roesler, A. (eds.), *Afar Depression of Ethiopia". Bad Bergzarben, F.R. Germany,* 38-54.

Bekele, B., 2012: *Review and reinterpretation of geophysical data of Tendaho geothermal field*. GSE, Addis Ababa, unpublished report, 96 pp.

Berckhemer, H., and Baier, B, 1975: Deep seismic sounding in the Afar region and on the highland of Ethiopia. *Proceedings of the International Symposium on the Afar Region and Related Rift Problems. Schweizerbart, I, Stuttgart,* 89-107.

Berdichevsky, M.N., and Dmitriev, V.I., 2002: *Magnetotellurics in the context of the theory of ill-posed problems*. Society of Exploration Geophysicists, USA, 215 pp.

Berktold, A., 1975: Magnetotelluric measurements in the Afar area. Afar Depression of Ethiopia. *Proceedings of the International Symposium on the Afar Region and Related Rift Problems, Schweizerbart, I, Stuttgart*, 262-275.

Cagniard, L., 1953: Basic theory of the magneto-telluric method of geophysical prospecting. *Geophysics, 18,* 605-645.

CNES Scientific Missions, 2015: Interaction with solar wind. CNES, webpage: *missions-scientifiques.cnes.fr/OVH/*

Craig, H., 1977: *Isotopic geochemistry and hydrology of geothermal waters in Ethiopian Rift Valley*. Scripps Institution of Oceanography, Isotopic Laboratory, report 77-14, 147 pp.

Dakhnov, V.N., 1962: Geophysical well logging. *Q. Colorado Sch. Mines, 57-2*, 445 pp.

Eysteinsson, H., 1998: *TEMRESD, TEMMAP and TEMCROSS plotting programs*. ÍSOR – Iceland GeoSurvey, unpublished programs and manual.

Flóvenz, Ó.G., Georgsson, L.S., and Árnason, K., 1985: Resistivity structure of the upper crust in Iceland, *J. Geophys. Res., 90-B12,* 10,136-10,150.

Flóvenz, Ó.G., Hersir, G.P., Saemundsson, K., Ármannsson, H., and Fridriksson, Th., 2012: Geothermal energy exploration techniques. In: Sayigh, A. (ed.), *Comprehensive Renewable Energy, 7.* Elsevier, Oxford, UK, 51-95.

Gonfiantini R., Borsi, S., and Ferrara, G., 1973: Isotopic composition of waters from the Danakil Depression, Ethiopia. *Earth and Planetary Science Letter, 18,* 13-21.

Groom, R.W., and Bailey, R.C., 1989: Decomposition of the magnetotelluric impedance tensor in the presence of local three-dimensional galvanic distortion. *J. Geophys. Res., 94*, 1913-1925.

Hailegiorgis, G., 2015: *Appendices to the report "Processing and joint 1D inversion of MT and TEM data from Alallobeda geothermal field in Tendaho, NE-Ethiopia".* UNU-GTP, Iceland, report 14 appendices, 106 pp.

Hersir, G.P., and Björnsson, A., 1991: *Geophysical exploration for geothermal resources. Principles and applications*. UNU-GTP, Iceland, report 15, 94 pp.

Hoversten, G.M. and Morrison, H.F., 1982: Transient fields of a current loop source above a layered earth. *Geophysics, 47,* 1068-1077.

Kearey, P., and Brooks, M., 1994: *An introduction to geophysical exploration* (2nd ed.). Blackwell Scientific Publ., London, 236 pp.

Kebede, Y., 2001: Application of the resistivity method in the Krísuvík geothermal area, Reykjanes Peninsula, SW-Iceland. Report 6 in: *Geothermal Training in Iceland 2001*. UNU-GTP, Iceland, 115-142.

Kebede, Y., Mengiste, A., Woldesemayet, B., Abera, F., Hailegiorgis, A.G., Dandir, K., and Mengesha, K., 2013: Magnetotelluric survey in Tendaho geothermal prospect North-East Ethiopia. Afar National Regional Government and GSE, Addis Ababa, unpubl. report.

Keller, G.V., and Frischknecht, F.C., 1966: *Electrical methods in geophysical prospecting*. Pergamon Press, NY, 527 pp.

Kidane, T., Courtillot, V., Manighetti, I., Audin, L., Lathittle, P., Quidelleur, X., Gillot, P.Y., Gallet, Y., Carlut, J., and Haile, T., 2003: New paleomagnetic and geochronologic results from Ethiopia Afar: Block rotations linked to rift overlap and propagation and determination of a ~ 2 Ma reference pole to stable Africa. *J. Geophys. Res*., 108 (B2), 10.1029/2001 JB000645.

Lahittle, P., Coulie, E., Mercier, N., Kidane, T., and Gillot, P.Y., 2001: K-Ar chronology and TL southern volcanism propagator for Red Sea Afar, since 300 ka, C.R. *Acad. Sci. Paris, Earth planet. Sci., 332*, (in French), 13-20.

Lahitte, P., Gillot, P.Y., and Courtillot, V., 2003a: Silicic central volcanoes as precursors to rift propagation: The Afar case. *Earth planet. Sci. Lett., 207*, 103-116.

Lahitte, P., Gillot, P.Y., Kidane, T., Courtilllot, V., and Abebe, B., 2003b: New age constraints on the timing of volcanism in central Afar, in the presence of propagating rifts, *J. Geophys. Res.,* 108 (B2), 2123.

Lemma Didana, Y., 2010: *Multidimensional inversion of MT data from Krýsuvík high-temperature geothermal field, SW-Iceland, and study of how 1D and 2D inversion can reproduce a given 2D/3D resistivity structure using synthetic MT data.* University of Iceland, Reykjavík, MSc thesis, UNU-GTP, report 4, 94 pp.

Lemma Didana., Y., Abera, F., Dendere, K., and Kebede, Y., 2012: *Magnetotelluric survey at Tendaho geothermal field in North East Ethiopia*. GSE, Addis Ababa, unpubl. report, 39 pp.

Mamo, T., and Bekele, B., 2014: Surface geological mapping at Tendaho geothermal field, Ethiopia. *Proceedings of the ARGeo-C5 Congress, Nairobi, Kenya,* 12 pp.

Megersa, G., and Getaneh, E., 2006: *Geological, surface hydrothermal alteration and geothermal mapping of Dubti-Semera area, Tendaho geothermal field.* GSE, Addis Ababa, unpubl. report, 66 pp.

Nure, K., 2001: *Gravity data interpretation of Gedemsa-Tullu Moye geothermal prospect area in the main Ethiopia rift (MER)*. GSE, Addis Ababa, unpubl. report, 48 pp.

Ofwona, C., 2010: Introduction to geophysical well logging and flow testing. *Presented at Short Course V on Exploration for Geothermal Resources, organized by UNU-GTP, GDC and KenGen, Naivasha, Kenya*, 6 pp.

Phoenix Geophysics, 2005: Data processing. User guide´s. Phoenix Geophysics, Ltd., Toronto.

Quist, A.S., and Marshall, W.L., 1968: Electrical conductances of aqueous sodium chloride solutions from 0 to 800°C and at pressures to 4000 bars. *J. Phys. Chem., 72,* 684-703.

Sky and Telescope, 2015: What is the solar wind? Sky and Telescope, webpage: *www.skyandtelescope.com/astronomy-resources/solar-wind/*

Simpson, F., and Bahr, K., 2005: *Practical magnetotellurics*. Cambridge University Press, Cambridge, UK, 254 pp.

Sternberg, B.K., Washburn, J.C., and Pellerin, L., 1988: Correction for the static shift in magnetotellurics using transient electromagnetic soundings. *Geophysics, 53-11,* 1459-1468.

Stimac, J., Armadillo, E., Rizzello, D., Mandeno, E., 2014*: Geothermal resource assessment of the Tendaho area.* Completed for UNEP and the Geological Survey of Ethiopia, report, 83 pp.

Teclu, A., and Mekonen, M., 2013: *Preliminary radon soil geochemical survey at Alallobeda geothermal prospect (Tendaho geothermal field).* GSE, GREAD, Addis Ababa, unpubl. report, 55 pp.

Teklemariam, M., and Kebede, S., 2010: Strategy for geothermal resource exploration and development in Ethiopia. *Presented at World Geothermal Congress*, *Bali, Indonesia*, 9 pp.

Teklesenbet Beyene, A., 2012: *Multidimensional inversion of MT data from Alid geothermal area, Eritrea; comparison with geological structures and identification of a geothermal reservoir*. University of Iceland, MSc thesis, UNU-GTP, report 1, 92 pp.

Tikhonov, A. N., 1950: The determination of electrical properties of the deep layers of the Earth´s crust (in Russian). *Dokl. Acad. Nauk. SSR 73*, 295-297.

Tikhonov, A. N., 1986: On determining electrical characteristics of the deep layers of the Earth´s. In Vozoff, K. (ed.), *Magnetotelluric methods*. Soc. of Expl. Geophys., 2-3.

UNDP, 1973: *Geology, geochemistry and hydrology of hot springs of the East African Rift System within Ethiopia*. UNDP, December report DD/SF/ON/11, NY.

Vozoff, K., 1972: The magnetotelluric method in the exploration of sedimentary basins. *Geophysics, 37,* 98-141.

Wolfenden, E., 2013: *Evolution of the southern Red Sea Rift: Birth of a magmatic margin.* Royal Holloway, University of London, PhD Thesis.